

THEORETICAL INVESTIGATION OF CO<sub>2</sub> ADSORPTION MECHANISM OVER (3-AMINOPROPYL)TRIMETHOXYSILANE-FUNCTIONALIZED MESOPOROUS SILICA SORBENTS



by

Berat Umay Topçubaşı

Submitted to Graduate School of Natural and Applied Sciences  
in Partial Fulfillment of the Requirements  
for the Degree of Master of Science in  
Chemical Engineering


Yeditepe University

2019

THEORETICAL INVESTIGATION OF CO<sub>2</sub> ADSORPTION MECHANISM OVER  
(3-AMINOPROPYL)TRIMETHOXY-SILANE-FUNCTIONALIZED MESOPOROUS  
SILICA SORBENTS

APPROVED BY:

Assoc Prof. Tuğba Davran Candan  
(Thesis Supervisor)  
(Yeditepe University)



.....

Assoc. Prof. Nihan Çelebi Ölçüm  
(Yeditepe University)



.....

Assoc. Prof. Mehmet Erdem Günay  
(Bilgi University)



.....

DATE OF APPROVAL: ..... / ..... / 2019

## ACKNOWLEDGEMENTS

First of all, I present my deep respectable thanks to Assoc. Prof. Tuğba Davran Candan who is instrumental in starting this study and during this period who is my academic advisor with unique researcher identity and also, who is emotional supporter with her mother identity.

Afterwards, I present my eternal love to partner of my life Serdar Topçubaşı, who has mobilized all his possibilities at all times with leaving her own expectations behind, throughout my undergraduate and graduate process. He has been my big power with his love and compassion for making real my dreams and goals and also, he is a unique father to our daughters with his big heart.

I present my sincere love and gratitude to my dear mother and father, who made the greatest effort to come to these days, always paved the way for me to be a researcher. All the goodness they brought me in our home was the main reason for me to have a good life.

I would like to thank my dear friends, Sezen Alsancak and Yeşim Çamlısoy. My university life was a huge adventure with their beggar description friendship. They has been my unique friends like a sister with their pure heartiness in all time.

The first name that spring to mind when calling Chemical Engineering department is Ezgi Baran who is our spiritual supporter. I owe she and my all teachers in our department dept gratitudes.

This work was supported by Yeditepe University within the scope of Yeditepe University Research Projects and Scientific Activities of Yeditepe University (YAP) “Project number YAP-LP-FEB-19007.

## ABSTRACT

### **THEORETICAL INVESTIGATION OF CO<sub>2</sub> ADSORPTION MECHANISM OVER (3-AMINOPROPYL)TRIMETHOXYSILANE-FUNCTIONALIZED MESOPOROUS SILICA SORBENTS**

Clarification of the interaction mechanism of CO<sub>2</sub> with the amine functionalized mesoporous silica sorbents is quite significant in the development of high-performance solid sorbents. This study aims to investigate the mechanism of CO<sub>2</sub> capture by (3-aminopropyl)trimethoxysilane (APTMS)-modified mesoporous silica by using DFT modeling. Two distinct models with differing size and surface amine density were employed for the study in order to elucidate the role of surface silanols on the reaction mechanism. Ammonium carbamate and carbamic acid were the two main adsorption products, carbamic acid being usually more stable and most likely being produced through the protonation of carbamate. Three types of carbamic acid were identified, each differing from one another in respect to the hydrogen bonding interactions involved in the structures. Direct participation of the surface silanols in the protonation/deprotonation steps of the mechanism was possible. However, our thermodynamic and kinetic considerations suggested that the role of surface silanols was more likely to stabilize the reaction species rather than being involved in the reaction mechanism directly.

## ÖZET

### **(3-AMİNOPROPİL) TRİMETOKSİSİLİAN İLE MODİFİYE EDİLMİŞ MEZOPORLU SİLİKA ADSORBANLARI ÜZERİNDE CO<sub>2</sub> TUTUNMA MEKANİZMASININ HESAPLAMALI OLARAK İNCELENMESİ**

Karbon dioksitin aminle modifiye edilmiş mezoporlu silika yapıları üzerindeki tutunma mekanizmalarının açıklığa kavuşturulması, yüksek performanslı katı adsorbanların geliştirilmesinde oldukça önemlidir. Bu çalışma, karbon dioksitin (3-aminopropil) trimetoksisilan (APTMS) ile modifiye edilmiş mezoporlu silika adsorbanları üzerindeki tutunma mekanizmalarının DFT modellemesi metoduyla araştırılmasını amaçlamaktadır. Çalışmada yüzeyde bulunan silanol yapılarının reaksiyon mekanizmasındaki rolünü aydınlatmak için farklı boyutlara ve yüzey amin yoğunluklarına sahip iki ayrı model kullanılmıştır. Hesaplamalarımız, karbon dioksitin daha çok amonyum karbamat ve karbamik asit olarak tutulduğunu, bunlardan karbamik asidin karbamata göre daha kararlı olduğunu ve karbamik asidin genellikle amonyum karbamat yapılarının protonasyonu yoluyla oluştuğunu ortaya koymuştur. Oluşan karbamik asit yapıları bünyelerinde barındırdıkları hidrojen bağları itibarıyla üç farklı gruba ayrılmıştır. Her ne kadar yüzeyde bulunan silanol yapılarının reaksiyon mekanizmasında aktif rol alabilecekleri gözlene de, bu mekanizmalar termodinamik ve kinetik açıdan incelendiğinde silanol yapılarının muhtemel görevinin tutunmada aktif rol oynamak yerine oluşan ara ve ana ürünleri stabilize etmek olduğu sonucuna varıldı.

## TABLE OF CONTENTS

ACKNOWLEDGEMENTS .....	ii
ABSTRACT .....	IV
ÖZET .....	V
LIST OF FIGURES .....	VIII
LIST OF SYMBOLS/ABBREVIATIONS.....	XII
1. INTRODUCTION .....	1
2. THESIS BACKGROUND.....	3
2.1. CARBON DIOXIDE CAPTURE .....	3
2.2. CARBON DIOXIDE ADSORPTION .....	6
2.2.1. Physical Adsorbents .....	6
2.2.2. Chemical Adsorbents .....	7
2.2.3. CO <sub>2</sub> Adsorption over Amine-Functionalized Mesoporous Silica .....	11
2.3. CARBON DIOXIDE CAPTURE MECHANISM.....	13
2.3.1. Absorption Mechanism .....	13
2.3.2. Adsorption Mechanism .....	14
2.4. MOLECULAR MODELLING .....	20
2.4.1. Density Functional Theory Method .....	22
2.4.2. Basis Sets.....	23
3. COMPUTATIONAL WORK.....	25
3.1. MOLECULAR MODELS .....	25
3.2. COMPUTATIONAL PARAMETERS.....	27
3.3. COMPUTATIONAL METHODOLOGY .....	28
4. RESULTS AND DISCUSSIONS.....	29
4.1. REACTION PATHWAY ANALYSIS OVER MODEL 5_5.....	29
4.1.1. Conformer 243 .....	29
4.1.2. Conformer 34 .....	31
4.1.3. Conformer 578 .....	33
4.1.4. Conformer 720 .....	35

4.1.5. Conformer 277 .....	38
4.1.6. Conformer 30 .....	41
4.1.7. General Consideration .....	46
4.2. REACTION PATHWAY ANALYSIS OVER MODEL 5_4_5.....	47
4.2.1. Conformer 254 .....	48
4.2.2. Conformer 287 .....	53
4.2.3. Conformer 473 .....	57
5. CONCLUSIONS AND RECOMMENDATIONS .....	62
REFERENCES .....	64



## LIST OF FIGURES

Figure 2.1. Schematic representation of the post-combustion, pre-combustion and oxy-fuel combustion.....	5
Figure 2.2. Schematic representation of MCM-41 molecular structure: (a) Hexagonal arrangement of pores [38], (b) Single pore.....	8
Figure 2.3. Schematic depiction of post-synthetic grafting.....	9
Figure 2.4. Commonly used organasilane structures I.....	10
Figure 2.5. Commonly used organasilane structures II.....	10
Figure 3.1. Molecular structures of (a) model 5_5 and (b) model 5_4_5.....	25
Figure 3.2. Molecular structure of 2 APTMS-MCM41(5_5).....	26
Figure 4.1. Molecular structures of (a) Model 243+CO <sub>2</sub> , (b) Physisorbed CO <sub>2</sub> , (c) Transition state, (d) Ammonium carbamate.....	29
Figure 4.2. Reaction energy diagram of CO <sub>2</sub> adsorption over conformer 243.....	30
Figure 4.3. Molecular structures of (a) Model 34+CO <sub>2</sub> , (b) Physisorbed CO <sub>2</sub> , (c) Transition state, (d) Carbamic acid I.....	31
Figure 4.4. Reaction energy diagram of CO <sub>2</sub> adsorption over conformer 34.....	31
Figure 4.5. Molecular Structures of Type-I Carbamic Acid.....	32
Figure 4.6. Molecular structures of (a) Model 578+CO <sub>2</sub> , (b) Physisorbed CO <sub>2</sub> , (c) Transition state, (d) Carbamic acid I.....	33



Figure 4.7. Reaction energy diagram of CO <sub>2</sub> adsorption over conformer 578.....	34
Figure 4.8. Molecular structures of (a) Model 720+CO <sub>2</sub> , (b) Physisorbed CO <sub>2</sub> , (c) Transition state 1, (d) Ammonium carbamate .....	35
Figure 4.9. Reaction energy diagram of CO <sub>2</sub> adsorption over conformer 720.....	36
Figure 4.10. Molecular structures of (a) Transition state 2, (b) Carbamic acid I obtained over conformer 720.....	36
Figure 4.11. Molecular structures of (a) Model 277+CO <sub>2</sub> , (b) Physisorbed CO <sub>2</sub> , (c) Transition state 1, (d) Carbamic acid I .....	38
Figure 4.12. Molecular Structures of Type-II Carbamic Acid .....	38
Figure 4.13. Molecular structures of (a) Transition state 2, (b) Carbamic acid II obtained over conformer 277.....	39
Figure 4.14. Reaction energy diagram of CO <sub>2</sub> adsorption over conformer 277.....	39
Figure 4.15. Molecular structures of (a) Model 30+CO <sub>2</sub> , (b) Physisorbed CO <sub>2</sub> , (c) Transition state 1, (d) Zwitterionic intermediate .....	40
Figure 4.16. Molecular structures of (a) Transition state 2, (b) Ammonium carbamate, (c) Transition state 3, (d) Carbamic acid II.....	41
Figure 4.17. Molecular structures of (a) Transition state 4, (b) Carbamic Acid I of reaction pathway I .....	42
Figure 4.18. Reaction energy diagram of CO <sub>2</sub> adsorption over conformer 30.....	43
Figure 4.19. Molecular structures of (a) Transition state 4, (b) Surface intermediate, (c) Transition state 5, (D) Carbamic acid III of reaction pathway II .....	44

Figure 4.20. Molecular Structures of Type-III Carbamic Acid .....	44
Figure 4.21. Molecular structures of (a) Model 254+CO <sub>2</sub> , (b) Physisorbed CO <sub>2</sub> , (c) Transition state 1, (d) Zwitterionic intermediate .....	48
Figure 4.22. Molecular structures of (a) Transition state 2, (b) Ammonium carbamate, (c) Transition state 3, (d) Carbamic acid II of reaction pathway I .....	49
Figure 4.23. Reaction energy diagram of CO <sub>2</sub> adsorption over conformer 254 .....	50
Figure 4.24. Molecular structures of (a) Transition state 2, (b) Surface intermediate, (c) Transition state 3, (d) Carbamic acid I of reaction pathway II .....	51
Figure 4.25. Molecular structures of (a) Transition state 3, (b) Carbamic acid III of reaction pathway III .....	52
Figure 4.26. Molecular structures of (a) Model 287+CO <sub>2</sub> , (b) Physisorbed CO <sub>2</sub> , (c) Transition state 1, (d) Zwitterionic intermediate .....	53
Figure 4.27. Molecular structures of (a) Transition state 2, (b) Ammonium carbamate, (c) Transition state 3, (d) Carbamic acid II of reaction pathway I .....	55
Figure 4.28. Reaction energy diagram of CO <sub>2</sub> adsorption over conformer 287 .....	55
Figure 4.29. Molecular structures of (a) Transition state 2, (b) Carbamic acid of reaction pathway II .....	56
Figure 4.30. Molecular structures of (a) Transition state 2, (b) Carbamic acid of reaction pathway III .....	56
Figure 4.31. Molecular structures of (a) Model 473+CO <sub>2</sub> , (b) Physisorbed CO <sub>2</sub> , (c) Transition state 1, (d) Zwitterionic intermediate over site I .....	57

Figure 4.32. Reaction energy diagram of CO <sub>2</sub> adsorption over conformer 473 (Site I).....	58
Figure 4.33. Molecular structures of (a) Model 473+CO <sub>2</sub> , (b) Physisorbed CO <sub>2</sub> , (c) Transition state 1, (d) Zwitterionic intermediate over site II.....	59
Figure 4.34. Reaction energy diagram of CO <sub>2</sub> adsorption over conformer 473 (Site II) ....	59
Figure 4.35. Molecular structures of (a) Transition state 2, (b) Carbamic acid II over site II for reaction pathway I.....	60
Figure 4.36. Molecular structures of (a) Transition state 2, (b) Carbamic acid over site II for reaction pathway II.....	60

## LIST OF SYMBOLS/ABBREVIATIONS

$E$	Electronic energy
$\hat{H}$	Hamiltonian operator
$E$	Matrix of orbital energies
$E_T$	Electrostatic (Kinetic) energy
$E_V$	Potential energy
$E_j$	Exchange energy
$E_{XC}$	Exchange-correlation functionals
$\Psi$	Wave function of the system
AEAPS	N-[3-(trimethoxysilyl)propyl]ethylenediamine
AMP	2-amino-2-methyl-1-propanol
APTES	3-aminopropyltriethoxysilane
APTMS	3-aminopropyl trimethyloxysilane
BP	Becke's parameter
B3LYP	Becke's three-parameter hybrid functional
CCS	Carbon capture storage
DEA	Diethanolamine
DFT	Density functional theory
DMAPS	3-(diethylamino)propyl]trimethoxysilane
FTIR	Fourier transform infrared spectrophotometer
GGA	Generalized gradient approximation
IR	Infrared spectroscopy
LDA	Local density approximation
MAPS	Methylaminopropyl trimethoxysilane
MEA	Monoethanolamine
MCM-41	Mobil composition of matter no.41
MD	Molecular dynamics
MDEA	N-methyldiethanolamine
MM	Molecular mechanics
MOF	Metal organic frameworks

NMR	Nuclear magnetic resonance
PEI	Polyethyleneimine
SBA-15	Santa Barbara Amorphous type material
STQN	Synchronous Transit-Guided Quasi-Newton
TEPA	Tetraethylenepentamine
QM	Quantum mechanics



## 1. INTRODUCTION

The dramatic increase in the level of atmospheric CO<sub>2</sub> since the industrial revolution has been accused of being the primary cause of global warming that is threatening our world. Post-combustion capture and subsequent sequestration of the emitted CO<sub>2</sub> in suitable geological formations have been considered as a potential near-term solution for preventing the climate change. The most conventional way of CO<sub>2</sub> capture is the chemical absorption by liquid amines. Even though the capture achieved by this method is effective and fast stemming from the chemical interaction of CO<sub>2</sub> with amines, this technology is still too expensive to be used in industrial scale mainly due to its energy-intensive and corrosive nature [1]. Accordingly, development of alternative methods that would effectively capture carbon dioxide at a lower cost is crucial for the remission of the effects of global warming.

Since evaporation of water during the regeneration step of the aqueous amine systems constitutes the highest amount of the total cost, utilization of solid sorbents for the capture of CO<sub>2</sub> has been proposed as an alternative and activated carbons, zeolites, and mesoporous silica have extensively been investigated for this purpose [2,3]. Although these materials were found to adsorb CO<sub>2</sub> quite successfully at low temperatures and elevated pressures, they do not function properly under the conditions of interest (~1 bar and ~75 °C) owing to their weak interactions with CO<sub>2</sub>. Thereupon, the idea of combining the best parts of these two methods, i.e. the low cost of solid adsorption systems and the chemical interaction between the amino groups and CO<sub>2</sub> of the aqueous amine systems, has emerged and amine-modified solid adsorbents have extensively been investigated as a promising alternative to the aqueous amine scrubbing method for the last years.

In the search for a stable, selective and high-capacity adsorbent with fast reaction kinetics, low cost, tolerance to moisture and mild regeneration conditions [2]; it is critical to clarify the interaction mechanism of CO<sub>2</sub> with the adsorbents. Despite of the considerable number of studies performed in the field, most of them were devoted to the improvement of the adsorption capacities and stabilities of these adsorbents as well as the inquiry of the effects of some structural properties on the adsorption performance [4-12]. Besides, in all those studies CO<sub>2</sub> adsorption mechanism over amine-based sorbents was accepted to be identical to that of aqueous amine systems- i.e. carbon dioxide was captured in the forms of

carbamates and bicarbonates- and the performance of the developed sorbents were evaluated accordingly [13]. Nonetheless, spectroscopic findings together with the results of a few DFT modeling studies reported the presence of products other than carbamates and bicarbonates indicating that the capture mechanism could totally be different in case of amine-functionalized sorbents underlying the necessity of mechanistic studies regarding CO<sub>2</sub> adsorption over amine-based sorbents [14-16].

In this work, quantum mechanical (QM) modeling of CO<sub>2</sub> adsorption over (3-aminopropyl)trimethoxysilane (APTMS) functionalized mesoporous silica was implemented with the objective of clarifying the capture mechanism of CO<sub>2</sub> over amine-modified mesoporous sorbents. 2 different sorbent models with varying number of free surface silanols and surface amine densities were used in order to examine the potential role of the hydrogen bonding network on the reaction mechanism, product stability and activation barriers.

Chapter 2 contains the theoretical background of the study together with a detailed literature survey on the CO<sub>2</sub> capture, while Chapter 3 provides the computational details involved in the study. The results obtained will be presented in Chapter 4 together with the corresponding discussions. Finally, Chapter 5 constitutes the basic conclusions derived from the study in addition to the recommendations for future studies.

## 2. THESIS BACKGROUND

### 2.1. CARBON DIOXIDE CAPTURE

The remarkable increase observed in the emissions of greenhouse gases beginning with the industrial revolution has resulted in one of the big environmental challenges of this century, the global warming. Carbon dioxide (CO<sub>2</sub>), the atmospheric concentration of which reached ~ 409 ppm by October 2019, is the main anthropogenic greenhouse gas and –as stated by the 5<sup>th</sup> assessment report of the Intergovernmental Panel on Climate Change (IPCC)– ongoing emissions will induce enduring changes in the climate system and further increments in the atmospheric temperature [17]. Hence, immediate action that would cut down the CO<sub>2</sub> emissions should be taken aiming to stabilize the atmospheric carbon dioxide concentration at around 450 ppm by the end of this century in order to mitigate the severe effects of the temperature increment.

Fossil fuel (coal, natural gas and petroleum) combustion comprises the biggest source of carbon dioxide emissions. According to the International Energy Agency statistics, electricity and heat generation alone created 42 percent of the total emissions in 2014 [18]. Even though the share of alternative energy sources like nuclear, solar and wind power is increasing day by day, fossil fuels are still the main source of energy constituting about 80 percent of the total energy generation. In this respect, carbon capture and storage (CCS)- which is mainly the capture of carbon dioxide from large point sources and its consecutive trapping in appropriate geological formations like depleted oil, gas and coal fields has emerged as a viable method for declining the anthropogenic emissions. CCS comprises of three main steps, i.e. CO<sub>2</sub> separation from flue gas, compression and transportation of the captured gas, and long-term trapping of the compressed gas in the proper geological formations. Separation of CO<sub>2</sub> from flue gas is the most expensive of all steps requiring further technological development before CCS can be used as an effective method for cutting down the carbon dioxide emissions [19].

There are three main methods, namely post-combustion, oxy-fuel combustion and pre-combustion, in use for CO<sub>2</sub> capture. As the name implies, in post-combustion capture, carbon dioxide is separated from the exit stream of a combustion chamber, which contains



CO<sub>2</sub> (10-15 percent), N<sub>2</sub> (70-75 percent), H<sub>2</sub>O (8-10 percent), O<sub>2</sub> (3-4 percent), SO<sub>x</sub> (trace amounts) and NO<sub>x</sub> (trace amounts) at ~75°C and atmospheric pressure [20]. In oxy-fuel combustion, since oxygen is separated from the air stream before it enters the combustion chamber, oxidation takes place under pure oxygen increasing the partial pressure of CO<sub>2</sub> significantly in the exhaust stream which in turn leads to a much easier carbon dioxide separation [19, 21]. Finally, in the pre-combustion capture, syngas (CO + H<sub>2</sub> + CO<sub>2</sub>) is obtained upon gasification of coal; CO is converted to CO<sub>2</sub> and H<sub>2</sub> in the presence of H<sub>2</sub>O through the water gas shift reaction and carbon dioxide is then separated from the H<sub>2</sub> stream [19, 21]. Even if the separation of CO<sub>2</sub> is much easier (due to the higher partial pressures of CO<sub>2</sub>) in case of pre-combustion and oxy-fuel combustion, post-combustion CO<sub>2</sub> capture is more extensively exploited since it can easily be integrated to the existing processes without requiring high investment costs [19]. A summary of the post-combustion, pre-combustion and oxy-fuel combustion is given in Figure 2.1.

CO<sub>2</sub> absorption by aqueous amine solutions (wet scrubbing) is the most developed and widely used technology for post-combustion capture. Although a vast number of amine structures were examined for their absorption performances, monoethanolamine (MEA) – which has been in use for more than 60 years– is by far the most broadly investigated amine structure, usually serving as a benchmark for the evaluation of the performances of other amines. Due to the strong chemical interaction of CO<sub>2</sub> with primary amines, MEA can effectively absorb CO<sub>2</sub> even under low partial pressures involved in post-combustion capture. However, such a strong chemical interaction results in a very high absorption energy for the final product (carbamate) which makes the regeneration of the solvent extremely energy intensive preventing the MEA-based capture systems to be used in large scale. In addition to the high regeneration cost, problems associated with corrosion and solvent degradation should also be overcome [19].

Other amine structures have extensively been investigated in order to find alternatives that would not suffer the above stated problems but capture CO<sub>2</sub> effectively and fast. Although, diethanolamine (DEA) and N-methyldiethanolamine (MDEA) –being less corrosive and volatile compared to MEA– seemed to have the potential, none of them were found to be superior to monoethanolamine [8, 9, 10, 11]. Sterically hindered amines, especially 2-amino-2-methyl-1-propanol (AMP), constitute another class of amines that have been very often under inquiry. Despite of their higher equilibrium capacity and lower product

stability (meaning lower regeneration energy) with respect to MEA, slow reaction kinetics associated with these types of amines limit their use as potential absorbers of CO<sub>2</sub> [22, 23, 24, 25]. Beginning with 1990s, various amine blends of MDEA [26, 27], AMP [23, 28] and piperazine [29, 30] with MEA came into play aiming to benefit from the advantages of each amine. However, none of the blends investigated had significantly improved performance that would contribute to the industrialization of the CO<sub>2</sub> capture. Alkyl amines with more than one amino group –like 2-(2-Aminoethylamino)ethanol [31], diethylenetriamine [32], triethylenetetramine [33] and tetraethylenepentamine [33]– have also been considered but despite of their higher absorption capacities and faster reaction kinetics, high degradation rates of them restrict their adoption in the field of CO<sub>2</sub> absorption.

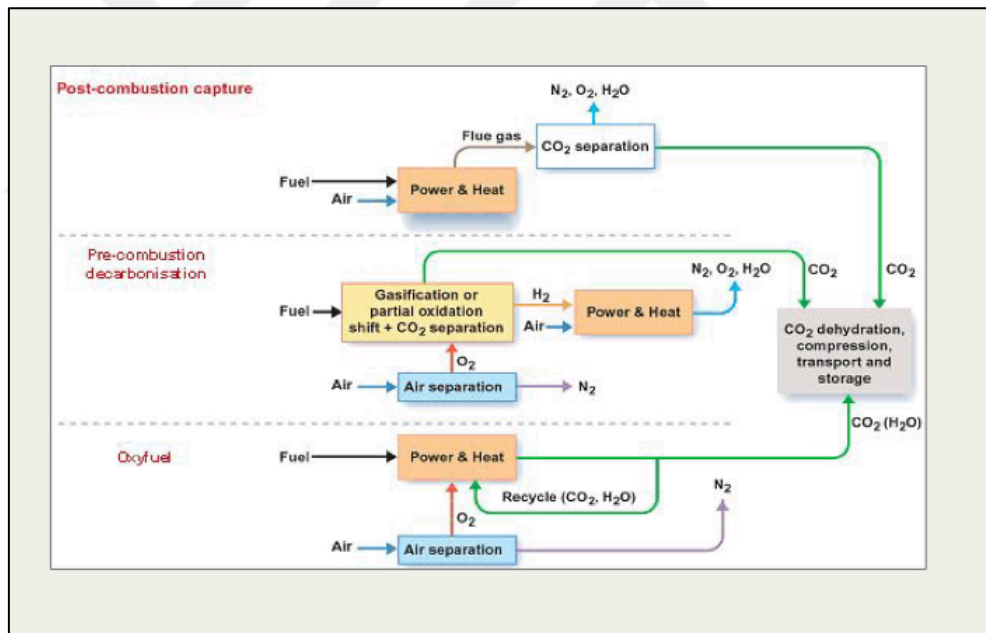


Figure 2.1. Schematic representation of the post-combustion, pre-combustion and oxy-fuel combustion [34].

As it is quite clear from the above discussion, aqueous amine absorption technologies are still much far away from achieving the required amount of reduction in CO<sub>2</sub> emissions; mainly because they are expensive, corrosive and environmentally unsafe (due to amine degradation). Accordingly, other methods that would eliminate the problems inherited in

wet scrubbing are sought and carbon dioxide adsorption by solid sorbents has attracted substantial attention as a potential alternative for CO<sub>2</sub> capture.

## **2.2. CARBON DIOXIDE ADSORPTION**

The energy-intensive nature of the aqueous amine absorption systems originates from the high stability of the absorption product as well as the huge amount of energy required for the heating and vaporization of the water involved within the system [19]. Consequently, when solid sorbents are employed for CO<sub>2</sub> capture rather than aqueous amines, water will be eliminated so that the energy requirement for the regeneration step will decline significantly and the corrosion problem will no more occur. However, CO<sub>2</sub> adsorption at low partial pressures and high temperatures (~75°C) is still a challenge; and a capture capacity of at least 2-3 mmol/g sorbent was stated as being necessary for the solid sorbents to compete with the conventional absorption technologies [35]. Both chemical and physical sorbents were considered in the search for an effective CO<sub>2</sub> capture process.

### **2.2.1. Physical Adsorbents**

In physical adsorption, species are trapped in the vicinity of the surface through weak van der Waals forces without being in a chemical interaction with the surface. Carbonaceous materials (such as activated carbon, graphene, and carbon nanotubes), zeolites and metal organic frameworks (MOFs) are the most frequently investigated physical sorbents for the adsorption of carbon dioxide.

Early examinations implemented on activated carbons displayed that adsorption performance of these materials were limited under flue gas conditions and deteriorated significantly in the presence of moisture [2]. Despite of the successive investigations aiming the enhancement of selectivity and capacity of these sorbents by increasing the surface area and pore size, CO<sub>2</sub> capture performance of these are still far below the required levels. Carbon nanotubes and graphene-based adsorbents were also under inquiry but they could not perform much better than the activated carbons under the conditions of interest [2].

Zeolites are crystalline and hydrated aluminosilicates with adjustable pore structures and adsorption characteristics [19]. Due to this tunable nature, they are very suitable for use as commercial adsorbents or catalysts. Although inspection of CO<sub>2</sub> adsorption by various forms of zeolites -in general- demonstrated that they were highly active, selective and stable under dry CO<sub>2</sub> flow when the pressure was high and temperature was low; a significant recession was observed in their performance (capacity, selectivity and stability) when the adsorption conditions were shifted to flue gas conditions [2,3].

MOFs are organic-inorganic hybrid materials composed of metal ions or clusters surrounded by organic linkers producing a repeating, cage-like structure that is highly porous. Since the pore structure of these materials can easily be modified to improve the adsorption performance by changing the organic or inorganic part, MOFs have extensively been under investigation for their CO<sub>2</sub> adsorption behaviors [19]. However, similar to the carbon-based materials and zeolites, their adsorption performances were poor under flue gas conditions [2, 36].

### **2.2.2. Chemical Adsorbents**

Physical adsorbents, despite of their lower regeneration energy, were shown to be improper for CO<sub>2</sub> capture under flue gas conditions stemming mainly from the weak interactions observed between CO<sub>2</sub> and the sorbent. Accordingly, the idea of combining the best parts of the two methods (adsorption and absorption), i.e. strong interaction of amines with CO<sub>2</sub> and smaller heat duties of regeneration in case of dry methods, was proposed and amine-functionalized solid sorbents have become quite popular in the search for a highly active, stable, and selective adsorbent for CO<sub>2</sub> with fast reaction kinetics and mild regeneration conditions [19].

Amine-based solid sorbents are created through the surface modification of physical adsorbents by amines. In addition to the adsorbents discussed in the previous section, mesoporous silica structures have often been in use as the support due to their high surface areas, well-ordered pore structures and much larger pore diameters with respect to activated carbons and zeolites [37]. Although modified synthesis procedures are also present, mesoporous silica structures are generally obtained through the polycondensation

of silica precursors around the quaternary ammonium surfactants that are used as templates [37]. These templates are then eliminated by calcination or extraction.

MCM-41 (Mobile Composition of Matter No. 41) and SBA-15 (Santa Barbara Amorphous type material) are the two most extensively studied mesoporous silica structures in the CO<sub>2</sub> adsorption literature. Both structures involve amorphous pore walls and two-dimensional hexagonal arrangements of pores, pores sizes being in the range of 1.5 nm - 10 nm for MCM-41 (Figure 2.2) and 4.6 nm – 30 nm for SBA-15 [38]. Nevertheless, pore sizes are highly tunable and illustrations of pore-expanded versions of both structures are present [8, 39].

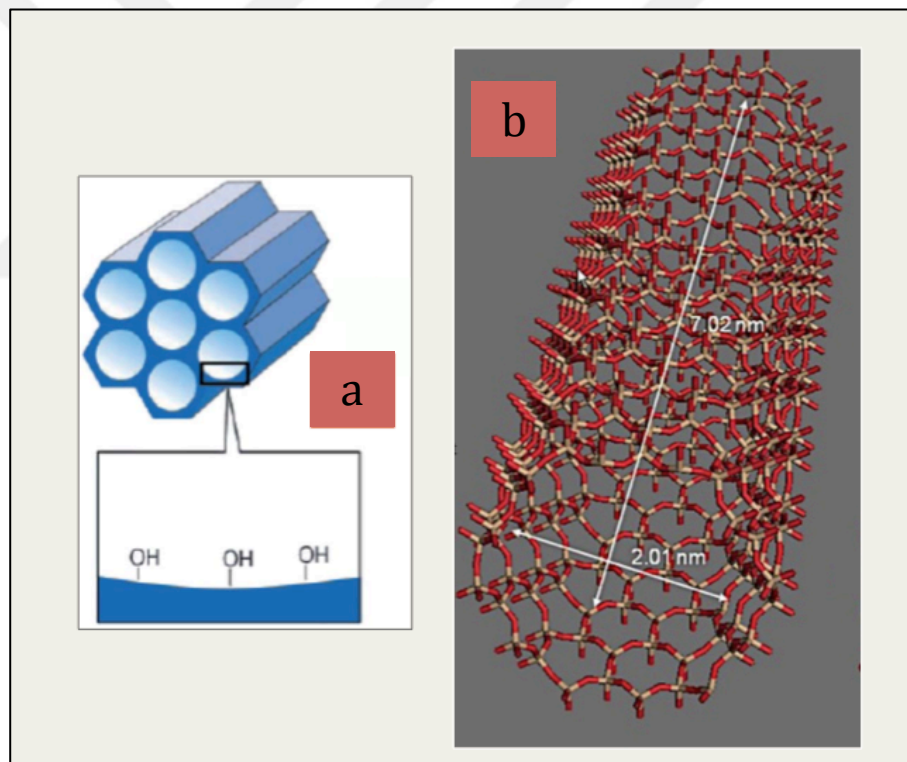


Figure 2.2. Schematic representation of MCM-41 molecular structure: (a) Hexagonal arrangement of pores [38], (b) Single pore [40].

Introduction of the amino groups onto the mesoporous silica is generally accomplished in two ways, namely impregnation and grafting. In impregnation, amine loading takes place through the sluggish van der Waals interplay between the surface and the amino groups upon the contact of the mesoporous silica with the amine solution, resulting in a densely-packed and randomly distributed aggregates of amine structures within the pores of the mesoporous silica [19, 41]. In post-synthetic grafting, on the other hand, amine tethering onto the surface is achieved through a condensation reaction between organosilanes and surface silanols, 3 silanols reacting with 1 silane compound (tridentate grafting) in ideal conditions to create chemically bonded organosilanes on the surface (Figure 2.3) [19, 42]. Organosilane structures commonly used for impregnation and grafting are given in Figure 2.4 and Figure 2.5.

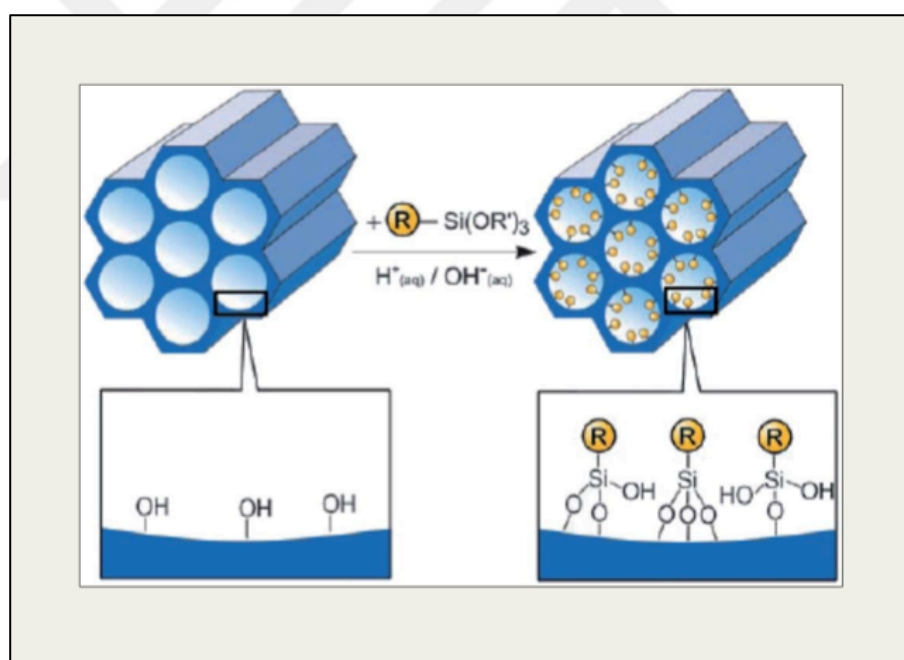


Figure 2.3. Schematic depiction of post-synthetic grafting [38].

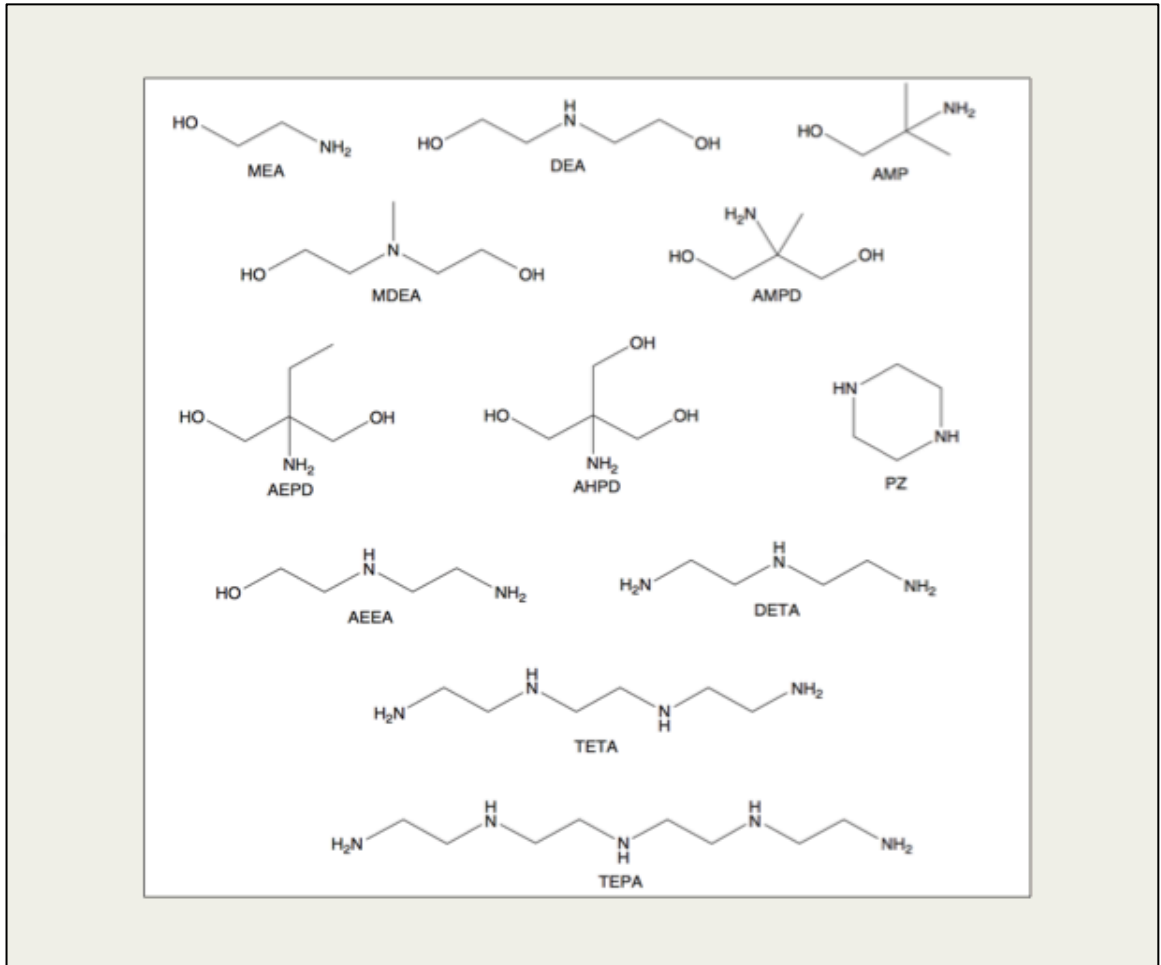


Figure 2.4. Commonly used organosilane structures I [9].

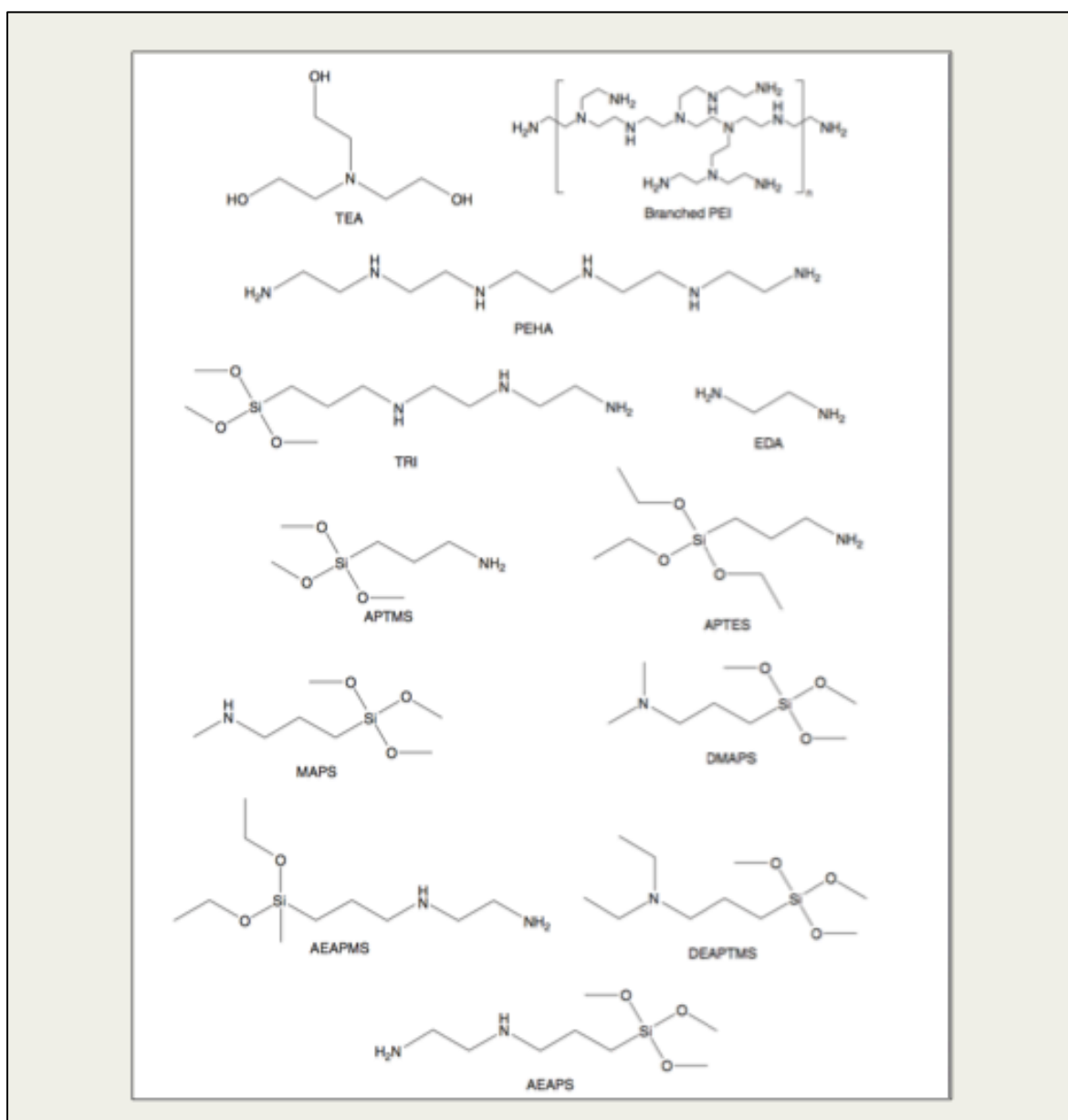


Figure 2.5. Commonly used organosilane structures II [19].

### 2.2.3. CO<sub>2</sub> Adsorption over Amine-Functionalized Mesoporous Silica

As it was stated above, amine-modified mesoporous silica sorbents have emerged as promising alternatives to the existing aqueous amine absorption technologies and an extensive amount of research has been carried out in the field up to now with the purpose of developing an effective CO<sub>2</sub> sorbent. Xu et al. were the first to discover a tremendous



increase in the adsorption capacity of a polyethyleneimine (PEI)-impregnated mesoporous silica compared to that of the bare support [43]. Investigations following this pioneering work mainly concentrated on the improvement of adsorption performances of these sorbents through an optimization of various parameters regarding the adsorption conditions, preparation methods and structures of the amines and mesoporous silica employed [44].

As for the adsorption conditions, effects of pressure, temperature and relative humidity on the CO<sub>2</sub> adsorption performance were inquired in order to develop the best sorbent for flue gas conditions. Experiments performed under various CO<sub>2</sub> partial pressures demonstrated that pressure dependence of adsorption capacity declined as the number of amine content increased due to the domination of chemisorption at higher amine contents [12, 44, 45]. Temperature, on the other hand, was shown to influence CO<sub>2</sub> uptake positively (up to 75°C) in the case of high-molecular-weight amines like TEPA, despite of the exothermic nature of adsorption [46, 47]. This was reported to be because of the kinetic barrier originating from the limited CO<sub>2</sub> diffusion experienced in densely-impregnated silica with bulky amine groups [44]. Finally, the impact of relative humidity was declared to change with the relative concentrations of CO<sub>2</sub> and H<sub>2</sub>O in the feed [48].

Adsorption experiments performed with various mesoporous silica (mostly MCM-41 and SBA-15) have shown that the type of silica did not affect the adsorption performance directly but through the pore volume and diameter [47, 49]. The influence of amine type was also studied by making use of various amine structures for modification aiming to determine the correlation between the amine structural properties (like the chain length, basicity, type of amino group (primary, secondary, tertiary), geometry (cyclic or linear), number of amine groups involved, surface amine density, etc.) and capture performance [11, 50]. Still, generalization of the results was not that easy as it was in the case of wet scrubbing technologies due to the existence of complicated relations between various parameters [44].

The impact of preparation methods on the uptake capacity was also frequently under inquiry. Since the amount of amine loading is restricted by the number of OH groups available at the surface in case of grafting, CO<sub>2</sub> adsorption capacity of these samples were found to be usually inferior with respect to that of the impregnated ones as CO<sub>2</sub> uptake is directly proportional to the amount of amine loading and the amine content of the grafted

samples is generally limited [12, 41, 44]. However, impregnated samples were not the best option either since they suffer from severe diffusion problems in case of high-molecular-weight amines and low thermal stability in case of low-molecular-weight ones [41, 51].

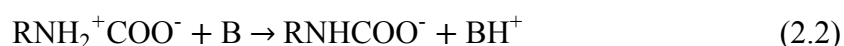
Although much of the effort was devoted to the measurement of capture performance as well as the optimization of various parameters to maximize this performance in case of adsorption, clarification of the CO<sub>2</sub> capture mechanism is equally critical for the development of effective capture technologies. Hence, literature findings regarding the capture mechanisms will be summarized in the following section.

## 2.3. CARBON DIOXIDE CAPTURE MECHANISM

### 2.3.1. Absorption Mechanism

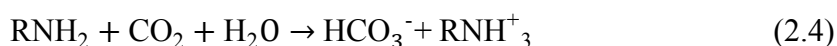
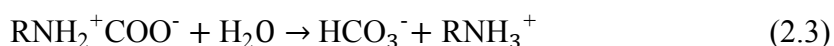
Acid-base reaction taking place between the acidic CO<sub>2</sub> and basic amine groups constitutes the basis of CO<sub>2</sub> absorption by aqueous amines, the mechanism of which has thoroughly been examined both by kinetic experiments and Density Functional Theory (DFT)-modelling studies [13, 19, 52-55].

According to the reported results, CO<sub>2</sub> is absorbed in the form of ammonium carbamates on condition that the amine is primary or secondary [13, 56]. The reaction pathway is known as the zwitterion mechanism and involves two steps. In the first step, CO<sub>2</sub> is attacked by the lone electron pair of the nitrogen giving rise to the production of the zwitterionic intermediate (Equation 2.1). This intermediate is then converted to an ammonium carbamate ion pair through deprotonation by a base molecule (Equation 2.2). This base molecule is usually another amine structure in the vicinity of the created zwitterion but it may also be a H<sub>2</sub>O molecule or OH<sup>-</sup> group.



When the amine is sterically hindered or tertiary, on the other hand, carbamate formation is either thermodynamically infeasible or cannot take place at all leading bicarbonate to be the final product [55, 57, 58]. Although it was previously suggested that bicarbonate was

formed through a two-step mechanism –zwitterion formation being the first step (Equation 2.1) and conversion of this zwitterionic intermediate into ammonium bicarbonate in the presence of water being the second step (Equation 2.3)–, one-step base catalyzed hydration mechanism (Equation 2.4) was much widely accepted later as being the bicarbonate formation mechanism [58].



As it is clear from the stoichiometry of the carbamate and bicarbonate formation reactions, 2 moles of amine molecules are required to capture 1 mole of  $\text{CO}_2$  in the case of carbamate formation, while the amine to  $\text{CO}_2$  ratio is 1:1 in the case of bicarbonate production. Despite of the higher equilibrium absorption capacity of bicarbonate production, use of tertiary and sterically hindered amines is limited due to the slow kinetics of bicarbonate formation, as it was discussed in Section 2.1.

### 2.3.2. Adsorption Mechanism

Although the interaction mechanism of  $\text{CO}_2$  with amines is quite clear in case of liquid-amine scrubbing, adsorption mechanism over amine-functionalized solid sorbents could not be fully addressed yet. Early studies assumed that  $\text{CO}_2$  was captured in the form of carbamates under dry conditions with a reaction stoichiometry of 1:2 ( $\text{CO}_2:\text{N}$ ), whereas bicarbonates were formed in the presence of water with a reaction stoichiometry of 1:1. Leal et al. provided spectroscopic evidence to this claim by reporting FTIR spectra for  $\text{CO}_2$  adsorption over 3-aminopropyl-triethoxysilane-grafted silica gel in the absence and presence of moisture [59]. FTIR frequencies identified at 1411 and 1385  $\text{cm}^{-1}$  were proposed to be carbamates and bicarbonates, respectively; while the 1596- $\text{cm}^{-1}$ -band was designated as the N-H bending frequency in ammonium. The changes observed in the relative intensities of the carbamate and bicarbonate bands as moisture was introduced into the system was interpreted as a further support for the assumption regarding the reaction mechanism. Subsequent studies performed with various amine-grafted mesoporous silica sorbents reported the presence of carbamates, bicarbonates and carbonates [60]. Huang et al. observed strong infrared bands at 1382, 1432 and 1485  $\text{cm}^{-1}$  [60]. The band at 1382  $\text{cm}^{-1}$

<sup>1</sup> was due to C-O stretching in bicarbonates whereas the next two were attributed to the asymmetric C-O stretches seen in carbamates. Formation of bidentate bicarbonate (band at 1634 cm<sup>-1</sup>), bidentate carbonate (bands at 1575 and 1390 cm<sup>-1</sup>), monodentate bicarbonate (bands at 1493 and 1432 cm<sup>-1</sup>), monodentate carbonate (band at 1337 cm<sup>-1</sup>) and carbamic acid (bands at 1595, 1440 and 1330 cm<sup>-1</sup>) were reported by Chang et al. in their in-situ infrared study of CO<sub>2</sub> adsorption over  $\gamma$ -(aminopropyl) triethoxysilane-grafted SBA-15 under humid conditions, where carbamic acid was claimed to be a precursor for the formation of protonated amine [61]. Khatri et al. identified bidentate bicarbonate species at 1628 cm<sup>-1</sup>, monodentate bicarbonate at 1470 and 1422 cm<sup>-1</sup>, monodentate carbonate at 1335 cm<sup>-1</sup>, bidentate carbonate at 1541 cm<sup>-1</sup>, and carbamic acid at 1287 cm<sup>-1</sup> in their combined study performed over [N-(2-aminoethyl)-3-aminopropyl]trimethoxysilane-grafted SBA 15 in the presence of water; monodentate bicarbonate, bidentate bicarbonate, and bidentate carbonate being claimed to be the main products of CO<sub>2</sub> capture [62]. Bidentate bicarbonate (1564 and 1373 cm<sup>-1</sup>), monodentate bicarbonate (1475 and 1409 cm<sup>-1</sup>) and monodentate carbonate (1313 cm<sup>-1</sup>) formation was reported over  $\gamma$ -(aminopropyl) triethoxysilane-grafted SBA-15 under humid conditions as well, subsequently by the same group [63]. Based on their observations of significant variations in the vibrational frequencies of adsorbed CO<sub>2</sub> species in the presence of H<sub>2</sub>O or D<sub>2</sub>O, it was argued that water played a critical role on the adsorption of CO<sub>2</sub>. On the contrary, Zheng et al. reported that the presence of 2 percent water had no effect on the capture and the adsorption of CO<sub>2</sub> over [N-(3-trimethoxysilyl)propyl]ethylenediamine-SBA-15 took place through the formation of intramolecular carbamate salts, which were claimed to be preferred over bicarbonates due to its fast kinetics [64]. Complementary findings that the presence of moisture had no influence on the amine-CO<sub>2</sub> interaction and the capture took place through the formation of alkylammonium carbamates were declared by Hiyoshi et al. via their infrared spectra obtained over N-methylaminopropyl trimethoxysilane, 3-aminopropyl triethoxysilane, N-(2-aminoethyl)-3-aminopropyl trimethoxysilane and (3-trimethoxysilylpropyl) diethylenetriamine-grafted SBA-15 [9]. It was also reported that no protonated amines were present at the surface in the absence of CO<sub>2</sub>, contrary to the previous claims [65, 66].

Although infrared spectroscopy has extensively been employed in the determination of interaction mechanism of CO<sub>2</sub> with amine-functionalized adsorbents, correct assignment of

the observed bands is not a straightforward task due to the strong overlap and low intensity of the bands, which in turn resulted in disagreements concerning the band assignments in the literature. Accordingly, the IR bands that were previously appointed as bicarbonates and carbonates were identified as various forms of carbamates later in the subsequent studies. Wang et al. investigated the interaction of CO<sub>2</sub> with polyethyleneimine (PEI)-functionalized SBA-15 by using in-situ transmission IR spectroscopy and DRIFTS under dry conditions and reported that alkylammonium carbamates (1410 cm<sup>-1</sup>) were the main reaction products of capture [67]. Formation of bicarbonates and carbonates was ruled out due to the absence of moisture despite of the observation of the strong bands at 1320, 1520, and 1650 cm<sup>-1</sup>, which were previously associated with bicarbonates and carbonates. The two broad bands arising at 2160 and 2450 cm<sup>-1</sup> upon carbon dioxide flow were, on the other hand, reported as chemically-adsorbed CO<sub>2</sub> species. A combination of alkylammonium carbamate (evidenced by N-H stretching at 3435 cm<sup>-1</sup>, N-H bending at 1626 cm<sup>-1</sup>, COO<sup>-</sup> asymmetric stretching at ~1545 cm<sup>-1</sup> and NH<sub>3</sub><sup>+</sup> bending at 1487 cm<sup>-1</sup>), carbamic acid (evidenced by C=O stretching of the carboxyl group at 1680 cm<sup>-1</sup>) and a third component that could not be clearly identified (observed at 1430 and 1330 cm<sup>-1</sup>) were claimed to be the reaction products of CO<sub>2</sub> with 3-(trimethoxysilyl)propylamine-functionalized mesoporous silica in the absence of water [68]. Similar findings related to the evolution of ammonium carbamates and hydrogen-bonded carbamic acids over (3-Aminopropyl) methyl-diethoxysilane and (3-aminopropyl) triethoxysilane-functionalized silica under anhydrous CO<sub>2</sub> flow were recorded by Bacsik et al. [69], the amount of ammonium carbamates being proportional to the surface amine density. In addition to these two products, formation of silylpropylcarbamates (probably through the slow reaction of carbamic acid with surface OH groups under extremely dry conditions) was also mentioned. Evolution of silylpropylcarbamates (surface-bound carbamates) was declared to be much slower compared to the former two products. Besides, even though the ammonium carbamates and hydrogen-bonded carbamic acids could easily be removed by dynamic vacuum, surface-bound carbamates were found to be quite stable to evacuation. No carbonates or bicarbonates were detected even under humid conditions; the enhancement observed in the adsorption capacity in the presence of moisture was associated to the additional ammonium carbamate ion pairs as well as the additional free amine groups liberated through the hydrolysis of silylpropylcarbamates [69]. Danon et al. investigated dry CO<sub>2</sub> adsorption over aminopropyl-triethoxy silane-grafted SBA-15 by

using FTIR and reported the presence of alkylammonium carbamates and silylpropylcarbamates in case of densely-loaded samples [70]. When a benzylamine spacer was employed in the synthesis to create isolated amine groups, surface-bound carbamate (silylpropylcarbamate) was the only product observed upon CO<sub>2</sub> flow, which was proposed to be formed through the interaction of an intermediate carbamate or carbamic acid with a surface silanol. Interestingly, in case of further capping of the surface silanol groups by making use of hexamethyldisilazane, no CO<sub>2</sub> adsorption took place indicating that surface OH groups are critical for the formation of silylpropylcarbamates. Different from the study of Bacsik et al., carbamic acid formation was claimed to be not occurring due to the instability of this species at room temperature.

Due to the disagreements concerning the identification of CO<sub>2</sub> capture products through IR spectroscopy, NMR spectroscopy has also been extensively used in the study of interaction of CO<sub>2</sub> with the amine-functionalized solid sorbents. Pinto et al. was among the first groups that investigated the activation and adsorption of CO<sub>2</sub> by 3-aminopropyltriethoxysilane (APTES)-grafted porous sorbents by using <sup>13</sup>CO<sub>2</sub> adsorption and solid-state NMR [71]. In addition to the peak observed at 125 ppm, which was attributed to the physisorbed CO<sub>2</sub>, three weak peaks at 43, 22, and 9 ppm (related to the propyl chain carbons in APTES) along with one strong resonance at 164 ppm were observed. Spectral deconvolution of the 164-ppm-peak resulted in two different resonances at 164 and 160 ppm, which were ascribed to carbamate and carbamic acid, respectively. Carbamic acid, being less stable, was argued to be produced by the interaction of CO<sub>2</sub> with an amine group and converted to alkylammonium carbamate through an interplay with another amine as long as the second amine is present in the vicinity of the formed carbamic acid. Moore et al. performed characterization of the CO<sub>2</sub> adsorption products obtained over hyperbranched amine polymers (HAS) that were formed by in-situ polymerization of aziridine monomers supported by SBA-15 using <sup>13</sup>CO<sub>2</sub> solid state NMR [72]. As a result of the occurrence of primary, secondary and tertiary amine groups within the structure of HAS polymers, a reaction mixture composing likely of carbamic acid, carbamates and an additional product that might be either bicarbonate or a different form of carbamate was detected. Another study carried out by Pinto group investigated the chemical adsorption of CO<sub>2</sub> over 3-aminopropyltriethoxysilane (APTES), trimethoxy[3-

(methylamino)propyl]silane (MAPS), ([3-(diethylamino)propyl]trimethoxysilane (DMAPS), and N-[3-(trimethoxysilyl)propyl]ethylenediamine

(AEAPS)-functionalized SBA-15 by using solid state NMR in conjunction with DFT modeling [14]. By employing primary (APTES), secondary (MAPS), tertiary (DMAPS) and diamine (AEAPS) structures together with varying surface amine densities, they objected to determine the effects of silica substrate (surface silanols mainly), chemical nature of the amine structure, intermolecular interaction between the surface amine groups as well as the surface amine density on the chemical adsorption products. Three  $^{13}\text{C}$  resonances, designated as A, B, and C, were observed in the region of 150-170 ppm upon  $\text{CO}_2$  flow over APTES and MAPS-modified mesoporous silica sorbents. The peak at  $\sim 153$  ppm was found to be existent only under extremely dry conditions and the species associated with this peak (A) was reported to be dominant at low amine coverages. DFT modeling calculations considered along with the NMR results revealed that species A was a carbamic acid, the OH group of which was not involved in any hydrogen bonding. Species B (resonating at 160 ppm) was demonstrated to be committed in very strong hydrogen bonding with the neighboring amines (between OH and  $\text{NH}_2$  of the neighboring amine) and was -in turn- reported to be a strongly hydrogen-bonded carbamic acid species. Species C that was detectable at 164 ppm, on the other hand, was determined to have hydrogen bonding between the  $\text{C}=\text{O}$  of the carbonyl group and a nearby amine as well as the C-OH of the species C and a surface silanol. Although this structure was reported to be compatible with an alkylammonium carbamate in a previous study of the same group [71], DFT calculations of this configuration indicated that the formation of a carbamate-ammonium pair was not favored thermodynamically.

In another study of  $\text{CO}_2$  adsorption over 3-aminopropyltrimethoxysilane (APTMS), MAPS and DMAPS functionalized SBA-15 performed by Foo et al., carbamic acid and carbamates were reported to be the two main chemisorption products in case of APTMS and MAPS [73]. APTMS carbamic acid was a monomer that was stabilized through hydrogen bonding with the surface silanols, while MAPS carbamic acid could be either a monomer (hydrogen bonded to a nearby amine) or a dimer (hydrogen bonded to the neighboring carbamic acid). As for the carbamate species, two different structures which differ from each other in terms of asymmetry were observed over APTMS-modified sorbents, whereas the one with lower asymmetry was predominant in case of MAPS-SBA-

15. DMAPS-functionalized samples, on the other hand, did not result in any carbamic acid or carbamate species, as expected. Bicarbonate, resulting from the residual water, was the only product that could be distinguished but it was in very small amounts.

Previous studies demonstrated that ammonium carbamate ion pairs could be formed only when the average distance between the neighboring amine groups is under a critical distance [74]. Cendak et al. performed a  $^{13}\text{C}$ -NMR-Chemical-Shift-Anisotropy study by tightly controlling the amine spacing in the APTES-SBA-15 samples employed with the purpose of elucidating the effect of amine spacing on the chemisorption of  $\text{CO}_2$  [75]. 3 samples, namely high-density ( $\sim 2.8$  mmol/g), low density ( $\sim 0.9$  mmol/g) and isolated-amine-involving ( $\sim 0.5$  mmol/g) APTES-SBA-15, were prepared and investigated by solid-state NMR under  $\text{CO}_2$  flow. 3 explicit resonances at 154, 160, and 164 ppm (designated as species A, B, and C, respectively in a previous study of the same group [14] were obtained, the relative concentration of each species being different for each sample. Species A, which is the dominant product in case of low-density and isolated-amine-involving samples, was previously associated with a paired carbamic acid, the OH group of which was not involved in any hydrogen bonding [14]. However, DFT results obtained for isolated carbamic acid models in this study were also in very good agreement with the experimental NMR results indicating that species A might also be an isolated carbamic acid possessing very weak interactions with the surface silanol groups [75]. In case of high-density samples, on the other hand, the major product was species C which was previously suggested to be a paired carbamic acid involving a strongly polarized hydrogen bond rather than being a completely deprotonated acid. Calculation of the asymmetry parameter for the three species observed, however, implied that species C was indeed more compatible with a propylammonium carbamate which was in opposition to the DFT results obtained with deprotonated models.

Identification of the  $\text{CO}_2$  chemisorption species, although it is quite critical for clarification of the capture mechanism, is not an easy task as it is quite clear from the above discussion. Recently, a critical inspection of all reported  $\text{CO}_2$  capture products of APTES-modified SBA-15 was performed by using solid-state NMR in combination with DFT modeling through a comparison of the experimental and theoretical NMR resonances as well as the infrared spectra [76]. Consideration of new ammonium carbamate models demonstrated that the resonance identified at 164 ppm (Species C) and associated previously with a



carbamic acid structure was indeed an alkylammonium carbamate that was stabilized by the surface silanol groups underlying the critical role of hydrogen bonding networks on the adsorption products once more.

#### **2.4. MOLECULAR MODELLING**

Molecular modeling, which is simply the science of numerical representation of molecular structures and simulation of their action by using classical and quantum physics, is widely used in the areas of catalysis, materials science, drug design, and etc. as a complement to experimental studies [77].

Molecular mechanics (MM) and molecular dynamics (MD) methods make use of the classical physics. In molecular mechanics, molecules are described as charged particles connected by springs and the energy of a molecule is estimated using an experimental energy function that is called a force field. Due to its simplicity, it can be employed to model even very big molecules without requiring high computation time. Even though the equilibrium geometries and conformations of molecules can be obtained through molecular mechanics, it may be regarded as being deficient in terms of explaining the chemical reactions since it provides no information about the electron distribution [78]. Molecular dynamics, on the other hand, simulates the motion of molecules within a given time period by solving numerically the Newton's equations of motion with the aim of acquiring the change observed in conformations of macromolecules with time [79].

Quantum mechanical models, on the contrary, are based on the quantum physics and describe molecules in terms of the interplays between the nuclei and electrons enabling the description of the electronic behavior of molecules by solving the quantum mechanical equations [78]. Although they provide more accurate results compared to molecular mechanics, their use for large molecules is restricted due to the high computational costs required by them.

Schrödinger equation is the fundamental equation of quantum mechanics that is used to find the allowed energy levels of atoms or molecules. The exact solution of this equation is possible only for the hydrogen atom; only approximate solutions can be attained for many-

electron atoms and molecules. The equation for a multi-nuclear and multi-electron system may be written as below (Equation 2.5).

$$\hat{H}\psi = E\psi \quad (2.5)$$

where,  $\hat{H}$  is the Hamiltonian operator,  $E$  is the electronic energy, and  $\Psi$  is the many-electron wave function describing the motion of electrons [80].

The Hamiltonian operator considers 5 contributions to the total energy of a molecule (Equation 2.6), namely the kinetic energies of the electrons and nuclei, the attraction of electrons by the nuclei, the interelectronic and internuclear repulsions [81].

$$\begin{aligned} \hat{H} = & -\frac{1}{2} \sum_i^{electrons} \nabla_i^2 - \frac{1}{2} \sum_A^{nuclei} \frac{1}{M_A} \nabla_A^2 \\ & - \sum_i^{electrons} \sum_A^{nuclei} \frac{Z_A}{r_{i,A}} + \sum_{i<j}^{electrons} \sum \frac{1}{r_{ij}} + \sum_{A<B}^{nuclei} \sum \frac{Z_A Z_B}{R_{AB}} \end{aligned} \quad (2.6)$$

The Hamiltonian given in Equation 2.6 involves pairwise attraction and repulsion terms meaning that particles move dependently with one another, which indeed complicates the problem. Born-Oppenheimer approximation uses the assumption that nuclei do not move based on the fact that motion of the nuclei is much slower than that of the electrons. In this way, the motion of electrons and nuclei is decoupled and electronic energies are estimated for fixed nuclear positions giving rise to the electronic Hamiltonian given in Equation 2.7 [81].

$$\hat{H}^{el} = -\frac{1}{2} \sum_i^{electrons} \nabla_i^2 - \sum_i^{electrons} \sum_A^{nuclei} \frac{Z_A}{r_{i,A}} + \sum_{i<j}^{electrons} \sum \frac{1}{r_{ij}} \quad (2.7)$$

Solution of the electronic Schrödinger equation is still intractable due to the interactions between individual electrons, so further simplification such that the motion of the electrons is completely independent from one another (Hartree-Fock approximation) is useful. This leads to a set of coupled differential equations, each involving the coordinates of a single electron. At this point, introduction of another approximation (Linear Combination of Atomic Orbitals) leads to the transformation of these equations into a set of algebraic equations which in turn simplifies the solution [80].

Exclusion of the electron-electron interactions in the Hartree-Fock model results in an overestimation of the electron-electron repulsion energy and in turn, the total energy. Correlated models like the density functional theory, configuration interaction and Moller-Plesset models have been developed to overcome this deficiency [82].

#### 2.4.1. Density Functional Theory Method

An approximate electron correlation term is included in this approach by making use of functionals of electron density. In this way, remarkably more accurate results are obtained without a significant increase in the cost of calculations with respect to the Hartree-Fock models. Electronic energy is partitioned into several terms:

$$E = E_T + E_V + E_J + E_{XC} \quad (2.8)$$

where,  $E_T$  is the kinetic energy originating from the electron motion,  $E_V$  is the electron-nucleus interaction energy,  $E_J$  is the electron-electron repulsion energy, and  $E_{XC}$  is the exchange-correlation energy including the remaining part of electron-electron interactions [80]. All components except for the kinetic energy are dependent on the total electron density ( $\rho$ ) that is given below (Equation 2.9).

$$\rho(r) = 2 \sum_i^{orbitals} |\psi_i(r)|^2 \quad (2.9)$$

$\psi_i$  being the commonly-named Kohn-Sham orbitals and the addition is performed over the electron pairs. Determination of the unknown orbital coefficients that would minimize the electronic energy results in a set of matrix equations called the Kohn-Sham equations, the solution of which will yield the ground-state density and in turn the ground-state electronic energy [80].

Among the components of electronic energy given in Equation 2.9, the exchange-correlation potential is not known analytically so approximations are required for its estimation. Depending on the approximations in use (like the local density approximation (LDA) or generalized gradient approximation (GGA)), three different classes of functionals may be discriminated, namely functionals based on LDA, functionals based on GGA, and functionals using the exact Hartree-Fock exchange. It should be noted that once the exchange-correlation functional is known exactly, then the DFT method will be exact [80, 83].

In most cases, DFT handles the problem in two parts. The first part that includes everything but the exchange-correlation functional is solved through the same analytical procedures involved in Hartree-Fock Models. Methods like BP and BLYP (which are known as pure density models) request only the Hartree-Fock Coulomb terms and are essentially much faster with respect to the Hartree-Fock models stemming from the special algorithms (based on multipole expansions) involved. The hybrid models like B3LYP, on the other hand, involve the Hartree-Fock exchange terms and their speeds are usually comparable to that of the Hartree-Fock models. The second part deals with the exchange-correlation functional, the analytical solution of which is still impossible as it was mentioned above [80].

#### **2.4.2. Basis Sets**

A basis set is a set (linear combinations) of functions used to represent the molecular orbitals of a molecule mathematically. Although Slater-type orbitals were in use in the early days due to their similarity to the eigenfunctions of the hydrogen atom, Gaussian-type functions are more frequently employed nowadays providing a much easier solution. To compensate for the loss of accuracy by using the Gaussian-type functions, linear combinations of these functions are used to set up the basis set [80].

STO-3G, consisting of functions required only to accommodate all of the electrons involved in the molecule, is the simplest possible representation of a molecule and is called the minimum basis set. Since STO-3G is atom centered and involve only spherical functions, this basis set is inadequate in defining the non-spherical molecules and the electron distributions.

Split-valance basis sets, which treat the core and valance electrons separately, were developed in order to overcome the first shortcoming. In 6-31G basis set, for example, 6 Gaussians are used to represent the core electrons; valance electrons are splitted in two as inner valance and outer valance electrons; 3 Gaussians are used for the inner valance electrons, while the outer valance electrons are represented by 1 Gaussian [80].

The second shortcoming was overcome by the introduction of polarization basis sets that provide d-type functions on main group elements and (optionally) p-type functions on hydrogen. 6-31G(d), for example, involves one set of d-functions added for the non-hydrogen atoms [80].



### 3. COMPUTATIONAL WORK

#### 3.1. MOLECULAR MODELS

Previous studies performed with various amine-modified sorbents demonstrated the critical role of the surface silanols as well as the surface amine density on CO<sub>2</sub> adsorption capacity [14, 73, 84, 85], claiming a lower uptake stemming from the restricted interaction of amines with the surface silanols in case of very-high-density sorbents [84]. Accordingly, 2 different models of (3-aminopropyl)trimethoxysilane (APTMS)-MCM-41 were employed in this study with the purpose of elucidating the impact of surface silanols and amine density on the reaction pathway of CO<sub>2</sub> adsorption.

As it was mentioned in Section 2.1.2, pore walls of the mesoporous MCM-41 is made of amorphous silica. Since DFT modeling of the whole MCM-41 is impossible due to the enormous size, two SiO<sub>2</sub> clusters that are compatible with the molecular structure of amorphous silica were used to represent the mesoporous silica. The smaller cluster, which was denoted as 5\_5 (Figure 3.1(A)), was made of two connected five-membered rings involving 8 SiO<sub>2</sub> units in total, whereas the larger one (5\_4\_5) (Figure 3.1(B)) was composed of two five-membered and one four-membered rings involving 10 SiO<sub>2</sub> units in total. Oxygen valences at the edges of the clusters were saturated with hydrogen atoms.

(3-aminopropyl)trimethoxysilane (APTMS) (Figure 2.5) is one of the most frequently employed amine structure with a primary amino group for the modification of mesoporous silica. APTMS-MCM-41 models were successively obtained by covalently binding two APTMS molecules on top of the each SiO<sub>2</sub> cluster through 3 Si-O-Si bonds, each reacting with 3 surface silanols and eliminating 3 water molecules through the condensation reaction. Molecular structure of the 2 APTMS-MCM-41 obtained with model 5\_5 is given in Figure 3.2.

Surface amine densities of the two models were estimated as 4.52 and 3.40 molecule/nm<sup>2</sup>, respectively for the smaller and larger models by dividing the number of APTMS molecules involved in the structure by the surface area of the mesoporous silica, surface

areas of each cluster being roughly calculated through the multiplication of the maximum Si-Si distances in the x and y directions.

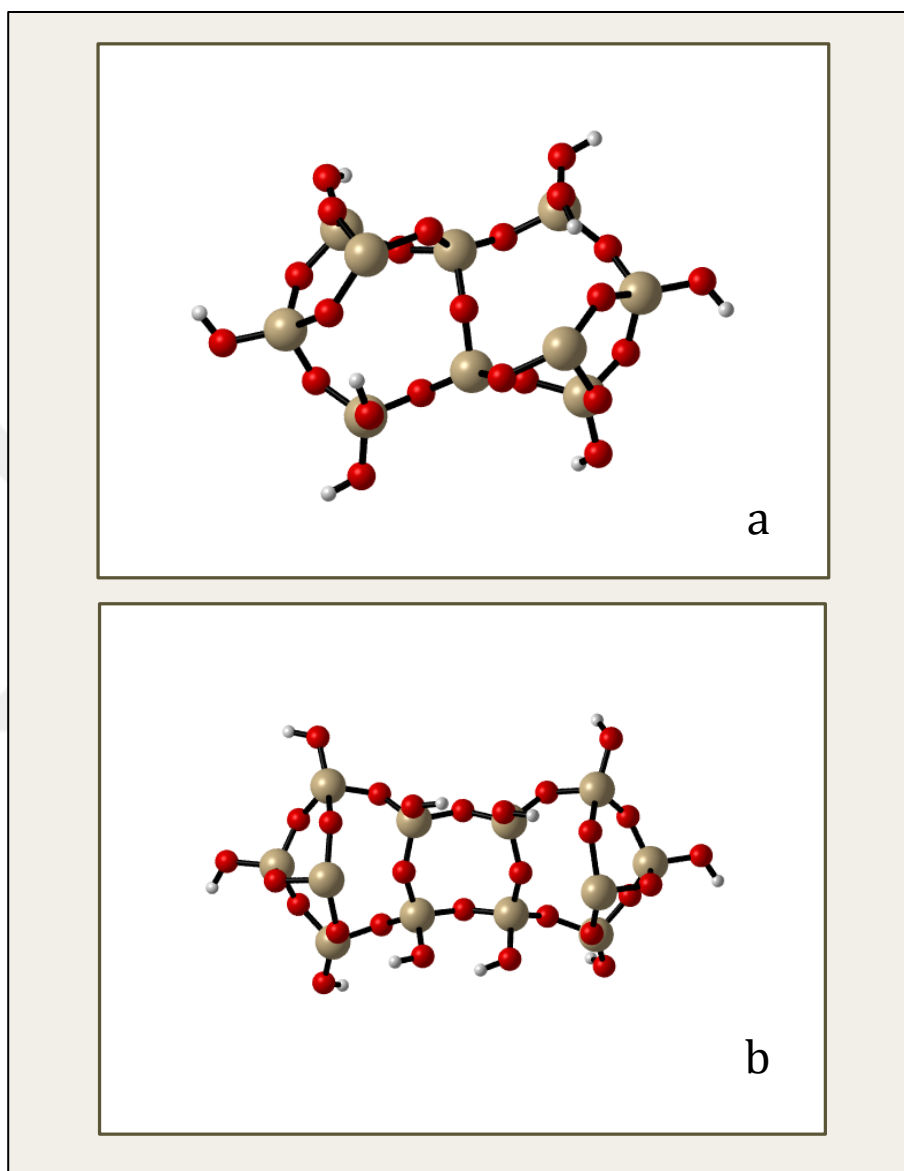


Figure 3.1. Molecular structures of (a) model 5\_5 and (b) model 5\_4\_5.

Conformer search of the two models were not carried out in this study. Molecular structures of the 729 conformers created for each of the models as a part of the graduation project executed by Yurdürün [86] were taken directly and the ones possessing nitrogen to nitrogen distances below 4 Å were chosen for further geometry optimization by DFT. Optimized conformers were then sorted with respect to their calculated energies; relative

energy of each structure was calculated with respect to the lowest-energy conformer and the ones having a relative energy less than 10 kJ/mol were selected for further investigation of the reaction pathway. Since two amine structures are required to capture one CO<sub>2</sub> according to the carbamate-formation mechanism, only the conformers with proper orientations of amines with each other were considered for mechanistic studies. Accordingly, models 243, 30, 34, 277, 578 and 720 were involved as the higher-amine density samples and models 254, 449 and 473 constituted the lower-density ones.

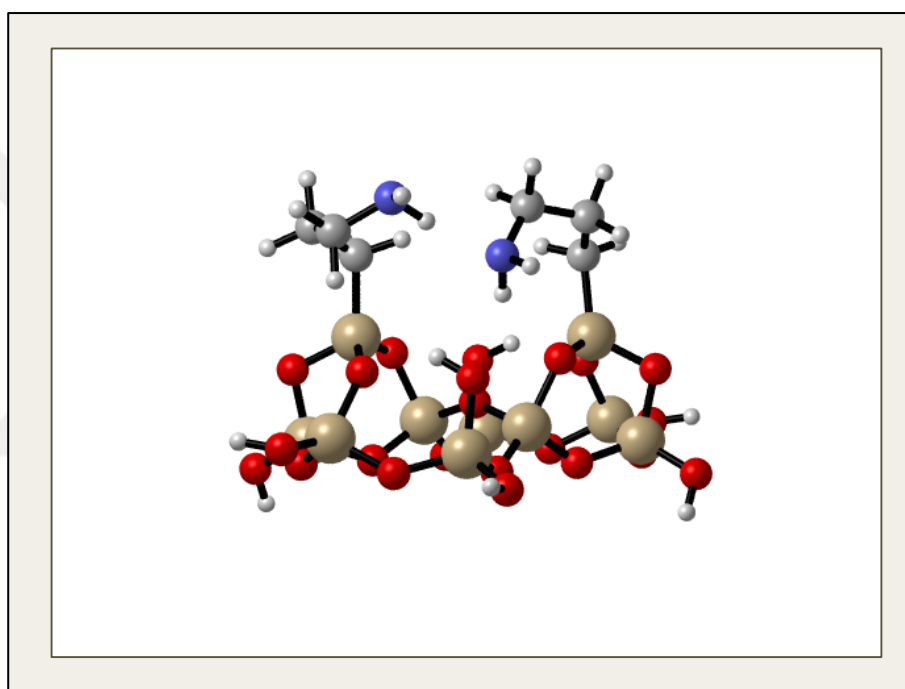


Figure 3.2. Molecular structure of 2 APTMS-MCM41(5\_5).

### 3.2. COMPUTATIONAL PARAMETERS

All the calculations regarding the investigation of reaction pathways were achieved by using the Density Functional Theory (DFT) method of Gaussian 16 [87], while the conformational search was executed through the “Conformer Search” tool of Avogadro 1.2.0 [88] that was based on molecular mechanics using the MMFF94 force field.

Becke’s three-parameter hybrid functional (B3LYP) [89] was employed as the exchange-correlation functional of DFT. Dispersive interactions were considered by applying



Grimme's D3 dispersion correction as included in Gaussian 16 [87]. As the basis set, the standard 6-31G(d) [90] with a single polarization function was employed.

### 3.3. COMPUTATIONAL METHODOLOGY

Investigation of the CO<sub>2</sub> adsorption pathway over APTMS-MCM-41 was initiated by the determination of the models that would be involved in the study. Three types of calculations, namely geometry optimizations, transition state searches and intrinsic reaction coordinate (IRC) calculations were implemented for the identification of the reaction mechanisms.

Geometry optimizations were used for the determination of the structures as well as the energies of the reactants, intermediates and products involved in the adsorption pathway, while QST2 option of the STQN (Synchronous Transit-Guided Quasi-Newton) method was exploited for the transition state searches. Since geometry optimizations seek to find the global minimum structures on the potential energy surface and transition state searches target saddle points of order 1, frequency calculations were performed subsequent to all optimizations with the purpose of confirming the nature of the obtained structure. On the other hand, even though most of the transition state searches result in saddle points of order 1, the nature of the deformation involved in the obtained transition state may be different from the desired one, implying the necessity of further confirmation of these structures. IRC calculations, which begin from the saddle point (transition state) and optimize the geometry of molecular structures involved along the reaction path in both directions (forward and reverse), were performed with this purpose [91]. Reaction energy diagrams are given in terms of Gibbs free energies rather than the electronic energies and Gibbs free energies are calculated using the thermochemistry data obtained through frequency calculations.

Finally, the two APTMS molecules involved in the selected models, the six Si-O-Si bonds binding these APTMS structures to the mesoporous silica, free silanol groups existing at the surface and CO<sub>2</sub> molecule (when available) were fully relaxed during all the calculations, while the coordinates of the remaining Si and O atoms were frozen in order to mimic the mechanical fixing provided by the vast amount of neighboring SiO<sub>2</sub> units present in real mesoporous silica sorbents.

## 4. RESULTS AND DISCUSSIONS

As mentioned in the previous section, 2 different models (5\_5 and 5\_4\_5) that differ from each other in surface amine densities and the number of free surface silanols involved in the model were employed for the study of CO<sub>2</sub> adsorption over APTMS-MCM-41. Accordingly, our findings will be discussed in two main sections, each being devoted to one of the selected models.

### 4.1. REACTION PATHWAY ANALYSIS OVER MODEL 5\_5

The smaller model had a surface density of 4.52 molecules/nm<sup>2</sup> and two free surface silanols remaining at the surface after functionalization. Estimated experimental surface amine densities for APTMS-modified MCM-41 sorbents were reported to be in the range of 1.12 to 4.42 molecules/nm<sup>2</sup> [44] indicating that the model with 4.52 molecules/nm<sup>2</sup> was a high-density sample.

As it was mentioned in the previous section, 6 different conformers –namely 243, 30, 720, 34, 277 and 578– were considered for the reaction pathway analysis. Even though the APTMS molecules did not align totally perpendicular to the MCM-41 surface in these structures originating from their high densities, their interaction with the free surface silanols were still restricted to some extent owing to both the orientation of the APTMS molecules and the limited number of available silanols.

#### 4.1.1. Conformer 243

Model 243 (Figure 4.1A) was estimated to be the lowest-energy conformer over which CO<sub>2</sub> adsorption was possible. Two amine groups interacted with each other through hydrogen bonding, which was likely the reason of the stability of the model. Among the two amine groups present, only N<sub>1</sub> was available for CO<sub>2</sub> capture since the lone pair on the other nitrogen was occupied by the hydrogen bonding interaction between N<sub>2</sub> and H<sub>20</sub>. CO<sub>2</sub> was found to be physically adsorbed over N<sub>1</sub> with an adsorption free energy of 4.9 kJ/mol. Estimated activation barrier for the conversion of this physisorbed CO<sub>2</sub> (Figure 4.1B) into

ammonium carbamate (Figure 4.1D) was  $\sim 69$  kJ/mol and ammonium carbamate product was calculated to be 69.6 kJ/mol less stable with respect to the reference structure (APTMS-MCM-41+CO<sub>2</sub>) indicating that the pathway was infeasible.

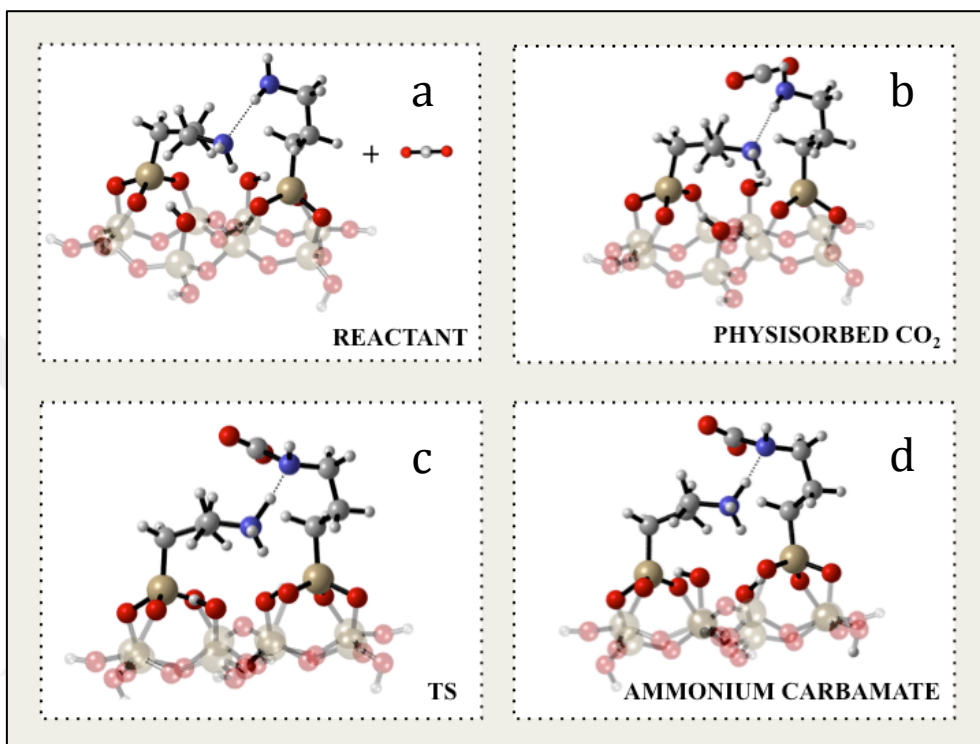


Figure 4.1. Molecular structures of (a) Model 243+CO<sub>2</sub>, (b) Physisorbed CO<sub>2</sub>, (c) Transition state, (d) Ammonium carbamate.

Reaction energy diagram concerning the carbamate formation over model 243 is presented in Figure 4.2. The instability of the obtained carbamate was mainly due to the absence of any hydrogen bonding interactions between the carbamate oxygens and the free surface silanols; the only interplay that the carbamate was involved was the hydrogen bonding between the H<sub>20</sub> of ammonium and N<sub>1</sub> of the carbamate.

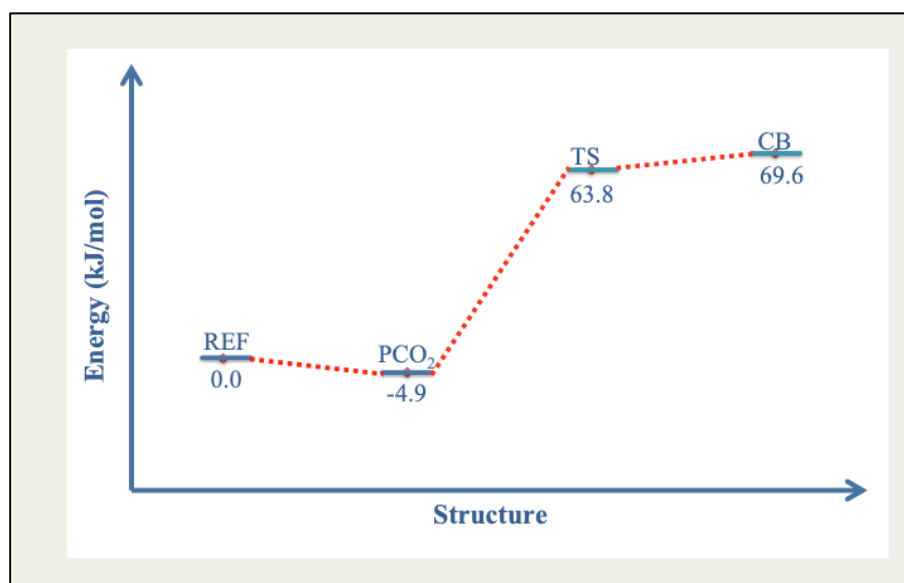


Figure 4.2. Reaction energy diagram of CO<sub>2</sub> adsorption over conformer 243.

#### 4.1.2. Conformer 34

Model 34 (Figure 4.3A) was 7.5 kJ/mol less stable than the conformer 243 and was similarly stabilized by the hydrogen bonding interactions between the two amine groups. Since the unpaired electrons over N<sub>1</sub> were in interplay with the hydrogen of the neighboring amine, only site N<sub>2</sub> was considered for CO<sub>2</sub> adsorption and the adsorption free energy was calculated as 3 kJ/mol.

According to the calculated mechanism (Figure 4.4), physisorbed carbon dioxide (Figure 4.3B) was subsequently transformed into a carbamic acid (Figure 4.3D) directly through the simultaneous transfer of proton (H<sub>23</sub>) from the CO<sub>2</sub>-bonded amine to the neighboring one (N<sub>1</sub>) and another proton (H<sub>20</sub>) from the neighboring amine (N<sub>1</sub>) to the nearest oxygen of the bonded CO<sub>2</sub>. The activation energy for this step was determined as ~67 kJ/mol, being comparable to that of the carbamate formation observed in the previous model. Carbamic acid, however, was 5 kJ/mol less stable than the reference compound (APTMS-MCM-41+CO<sub>2</sub>) so that its formation was thermodynamically not feasible. Nevertheless, significant stabilization of the product with respect to the carbamate observed over model 243 through the hydrogen bonding between the -COH of carbamic acid and the -NH<sub>2</sub> of the neighboring amine was noticeable.

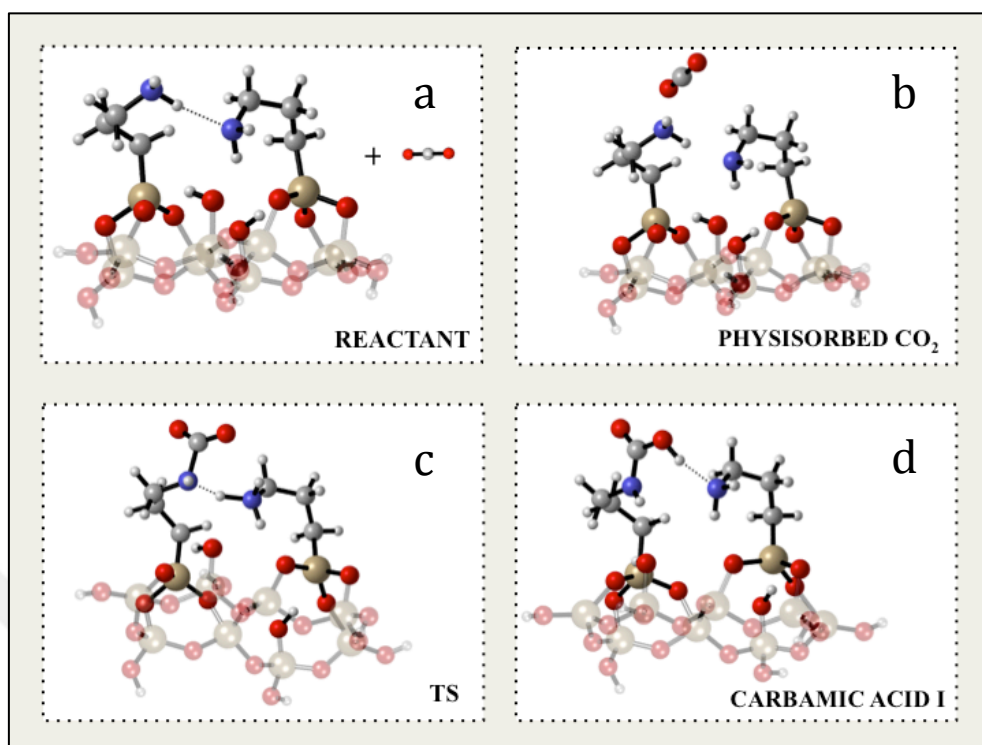


Figure 4.3. Molecular structures of (a) Model 34+CO<sub>2</sub>, (b) Physisorbed CO<sub>2</sub>, (c) Transition state, (d) Carbamic acid I.

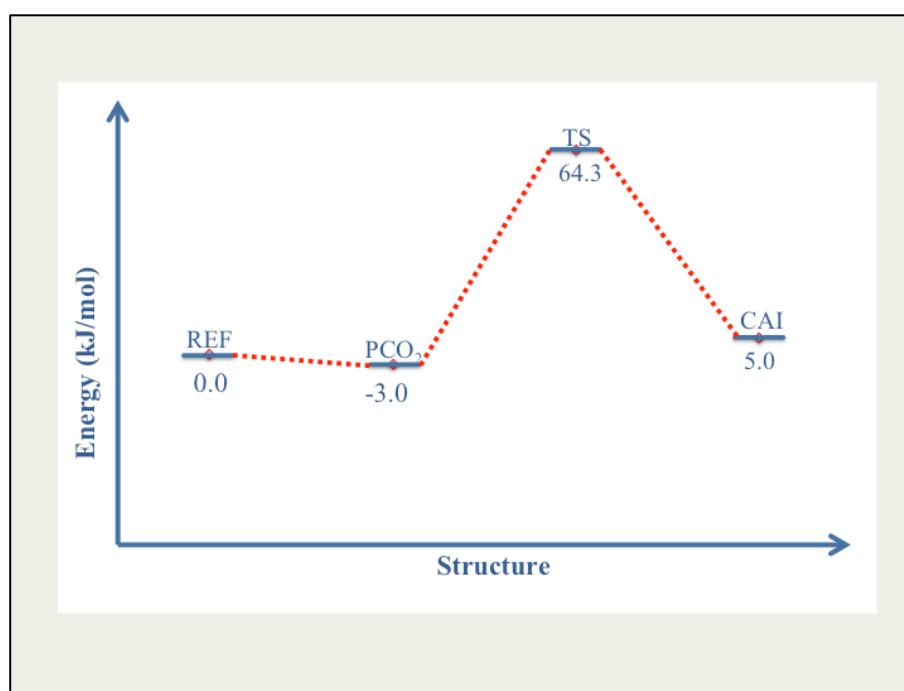


Figure 4.4. Reaction energy diagram of CO<sub>2</sub> adsorption over conformer 34.

The interaction between the OH of the acid and the nitrogen of the neighboring amine was the only hydrogen bonding involved in the structure of this carbamic acid, which was designated as type I (Figure 4.5). Previous findings reported the presence of a number of different carbamic acid structures varying from one another in their stabilities and the hydrogen bonding network that they are involved in based on NMR findings [76]. Although, the carbamic acid observed here was at first sight thought to be the species A reported previously by Pinto et al. [71], that structure was later suggested to be an isolated carbamic acid which was not involved in any hydrogen bonding through its -COH group [76]. The carbamic acid observed here was, however, not isolated and hydrogen bonded to the neighboring amine through the -COH.

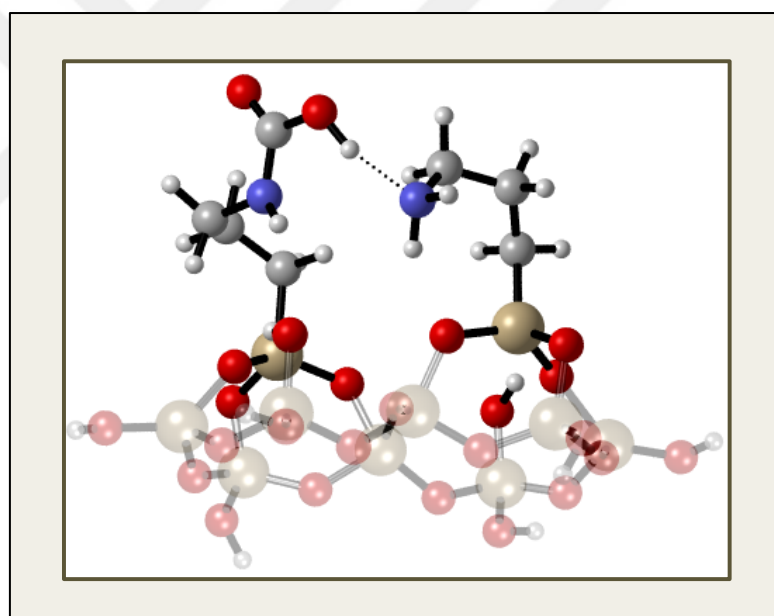


Figure 4.5. Molecular Structures of Type-I Carbamic Acid.

#### 4.1.3. Conformer 578

Conformer 578 (Figure 4.6A) was 9.8 kJ/mol less stable than the lowest energy conformer and was in interaction with the neighboring amine similar to the previous models. Only site  $N_1$  was considered for  $CO_2$  adsorption due to the unavailability of the other nitrogen

originating from the interaction between the two amino groups. An identical pathway that resulted in the direct production of type I carbamic acid (Figure 4.6D) from physisorbed  $\text{CO}_2$  (Figure 4.6B) was observed over conformer 578. Adsorption free energy of  $\text{CO}_2$  was calculated as 7.4 kJ/mol, while the reaction barrier for the carbamic acid formation was 70 kJ/mol. Similar to the previous case, formation of the final product was unfavorable with a relative free energy of 6.8 kJ/mol with respect to the reference state (APTMS-MCM-41+ $\text{CO}_2$ ).

The only hydrogen bonding interaction that the structure was involved in was through the OH of the acid. The schematic representation of the observed reaction pathway is given in Figure 4.7, while the molecular structures involved in the pathway may be found in Figure 4.6.

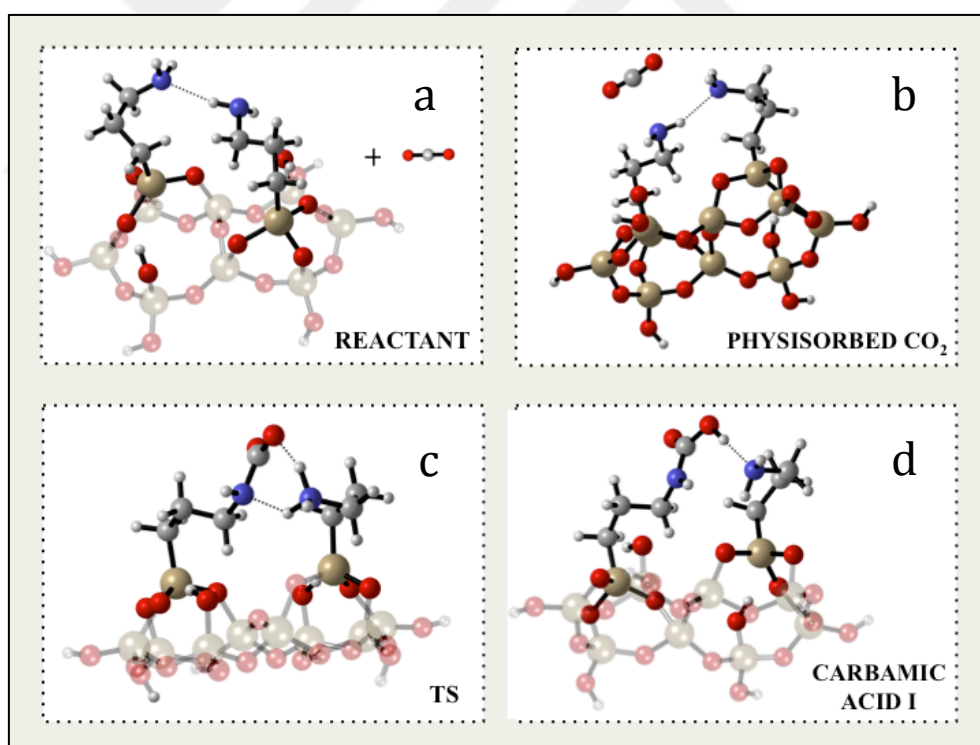


Figure 4.6. Molecular structures of (a) Model 578+ $\text{CO}_2$ , (b) Physisorbed  $\text{CO}_2$ , (c) Transition state, (d) Carbamic acid I.

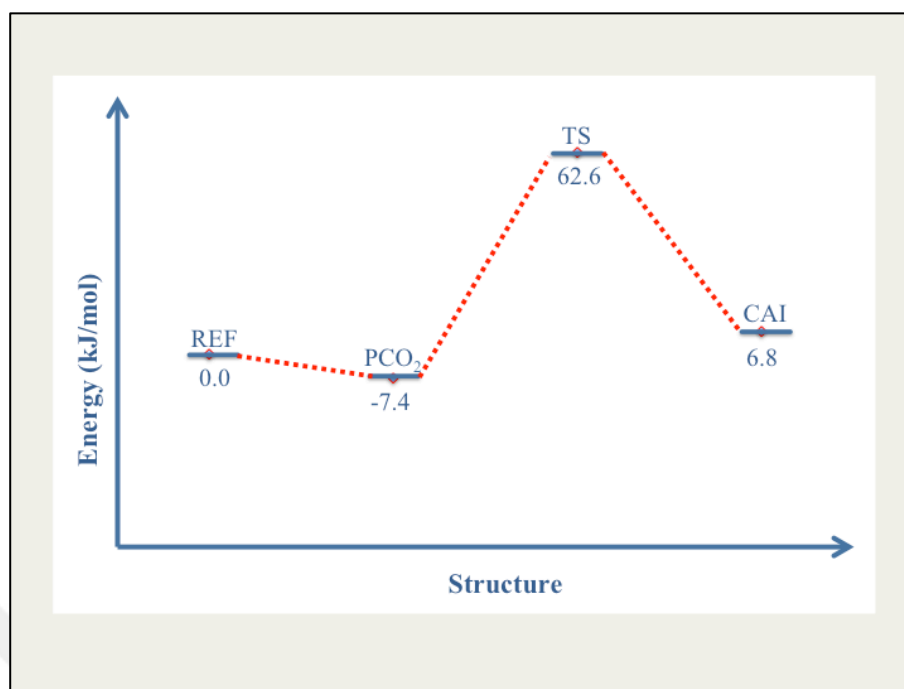


Figure 4.7. Reaction energy diagram of CO<sub>2</sub> adsorption over conformer 578.

#### 4.1.4. Conformer 720

Conformer 720 (Figure 4.8A) was 4.6 kJ/mol less stable with respect to the lowest-energy conformer and it involved a similar interaction between the two amine groups as the previous models. N<sub>1</sub> was the only available site for CO<sub>2</sub> adsorption and the free energy of adsorption was estimated as 0.7 kJ/mol.

According to the reaction pathway observed (Figure 4.9), CO<sub>2</sub> was subsequently converted to ammonium carbamate (Figure 4.8D) through the deprotonation of the CO<sub>2</sub>-bonded amine by the neighboring amino group, the activation energy being ~75 kJ/mol. The ammonium ion was hydrogen bonded to the nitrogen of the neighboring amine, to the oxygen of the carbamate and to the surface oxygen involved in the Si-O-Si bridge. Despite of this hydrogen bonding network, formation of carbamate was determined to be endothermic with a relative energy of ~ 78 kJ/mol relative to the reference state (APTMS-MCM-41+CO<sub>2</sub>). Owing to the interaction between the oxygen of the carbamate and hydrogen (not the one acquired by protonation but another one) of the ammonium, this



carbamate was further protonated leading to the formation of a carbamic acid (Figure 4.10B) that was hydrogen bonded to the neighboring amine through the OH group (type I). The reaction barrier calculated for the conversion of carbamate to carbamic acid was just 1.5 kJ/mol indicating that the proton transfer was facile. Formation of the final product, despite of being a type I carbamic acid, was estimated to be exothermic with a relative energy of 9.7 kJ/mol with respect to the reference structure (APTMS-MCM-41+CO<sub>2</sub>). Molecular structures of all the species included in the mechanism are presented in Figure 4.8 and 4.10.

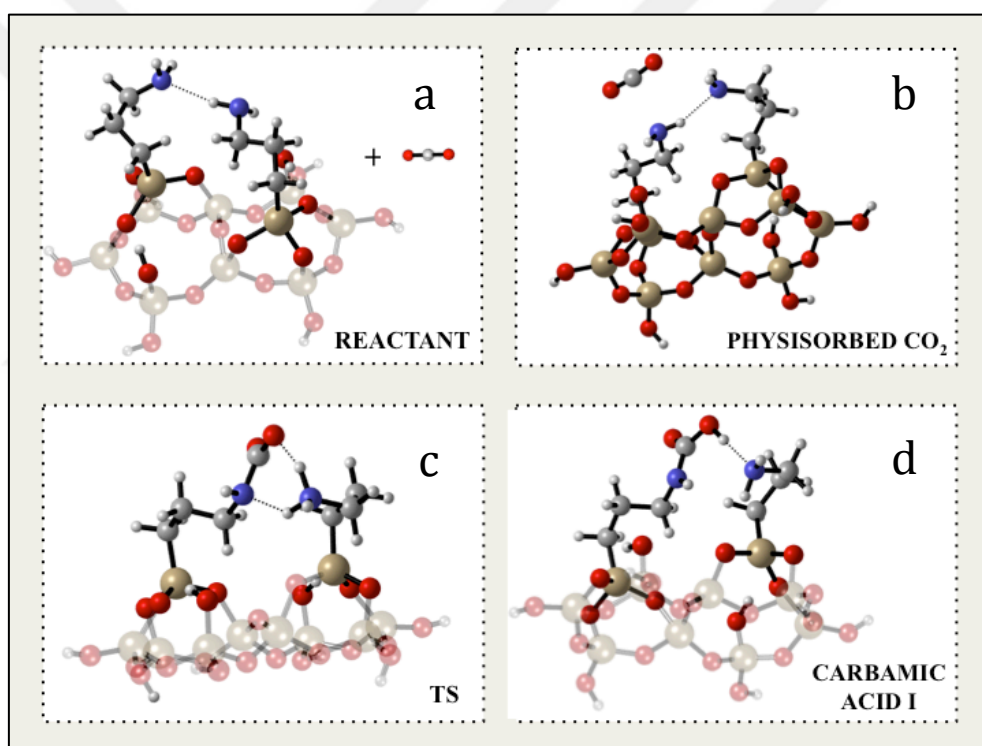


Figure 4.8. Molecular structures of (a) Model 720+CO<sub>2</sub>, (b) Physisorbed CO<sub>2</sub>, (c) Transition state 1, (d) Ammonium carbamate.

Reaction pathways observed for conformer 720 and conformers 34 and 578 indeed proceeded through a similar exchange of protons, i.e. CO<sub>2</sub>-bonded amine loses one proton to the neighboring amine and the neighboring amine loses one proton (different from the gained one) to the carbamate, and resulted in the same end products (type I carbamic acid).

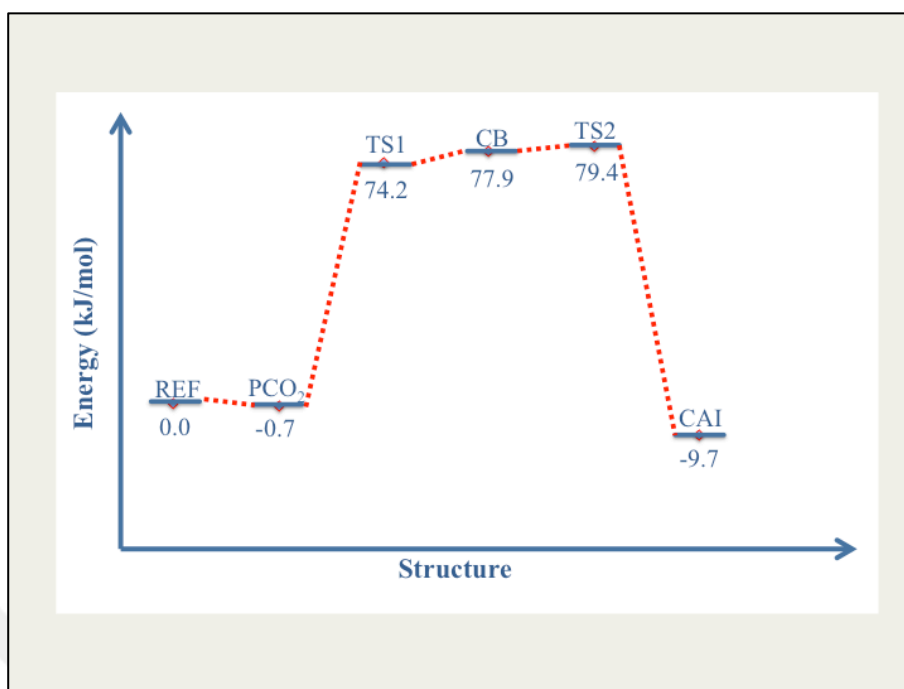


Figure 4.9. Reaction energy diagram of CO<sub>2</sub> adsorption over conformer 720.

The only difference between the two mechanisms was that this exchange took place simultaneously in case of conformers 34 and 578 whereas it occurred in two steps in case of conformer 720.

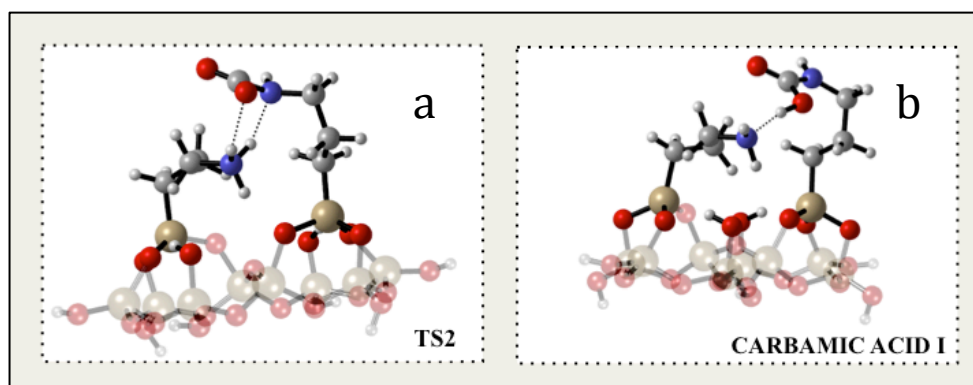


Figure 4.10. Molecular structures of (a) Transition state 2, (b) Carbamic acid I obtained over conformer 720.

#### 4.1.5. Conformer 277

Conformer 277 (Figure 4.11A) had a relative energy of 7.6 kJ/mol with respect to the lowest-energy conformer. Due to the proximity of the two amine groups, they were in interaction with each other and  $N_1$  was the more available site for  $CO_2$  adsorption.

Adsorption of  $CO_2$  over site  $N_1$  –which was followed by the transformation of it into a type I carbamic acid– was found to be quite weak (0.9 kJ/mol). Direct conversion of physisorbed  $CO_2$  (Figure 4.11B) into carbamic acid (Figure 4.11D) required an activation barrier of  $\sim 80$  kJ/mol, being comparable to the values obtained for conformers 34 and 578. Different from the previous cases, however, formation of this carbamic acid was feasible with an energy of -17.8 kJ/mol relative to the reference state (APTMS-MCM-41 +  $CO_2$ ). Due to being a type I carbamic acid, OH of the acid was hydrogen bonded to the nitrogen of the neighboring amine but unlike the previous cases, one of the hydrogens of the neighboring amine was in the proximity of the -CO of the carbamic acid, NHO angle being equal to  $125.7^\circ$  and H-O distance being 2.2 Å (Figure 4.11D), indicating an additional but weaker hydrogen bond interaction stabilizing the observed carbamic acid. This product was then observed to be converted into another carbamic acid structure (Figure 4.13B) with an activation energy of 14.3 kJ/mol. Transformation of type I carbamic acid took place through the simultaneous transfer of the carbamic acid proton to the neighboring amine and another proton of the neighboring amine to the -CO group of the acid.

The activation barrier calculated for this step was 14.3 kJ/mol and the resulting, new carbamic acid was found to be 32.4 kJ/mol more stable relative to the reference point (APTMS-MCM-41+ $CO_2$ ). This structure was named as type II carbamic acid (Figure 4.12) and was involved in hydrogen bonding interactions with the neighboring amine as well as the free surface silanol through the -OH and -CO groups, respectively. The molecular structures of the species observed along the pathway and schematic representation of the reaction pathway are presented in Figures 4.11, 4.13, and 4.14, respectively.

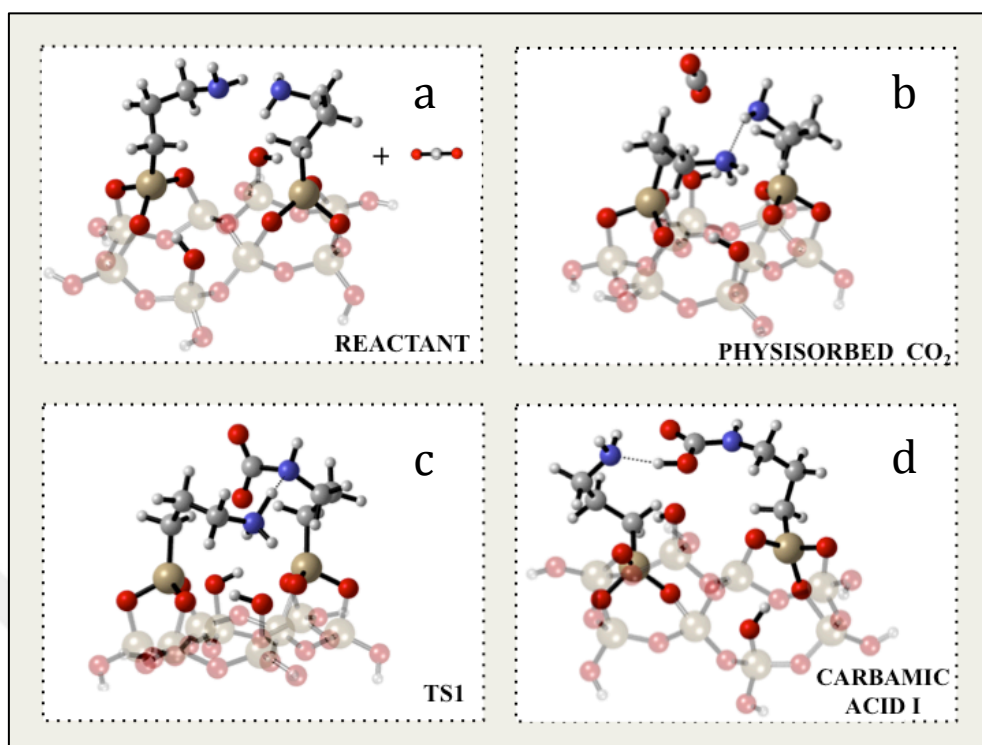


Figure 4.11. Molecular structures of (a) Model 277+CO<sub>2</sub>, (b) Physisorbed CO<sub>2</sub>, (c) Transition state 1, (d) Carbamic acid I.

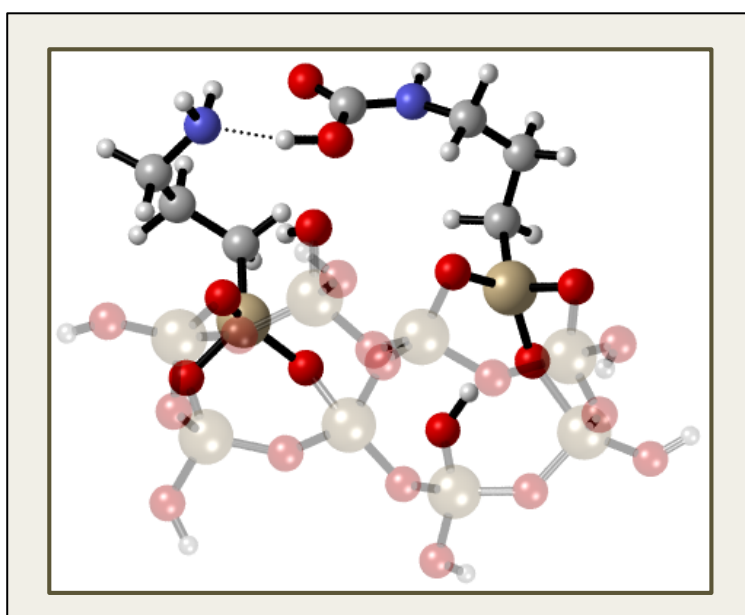


Figure 4.12. Molecular Structures of Type-II Carbamic Acid.

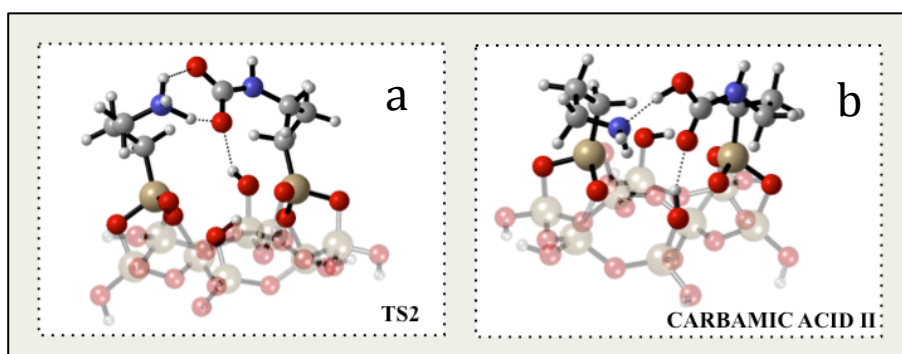


Figure 4.13. Molecular structures of (a) Transition state 2, (b) Carbamic acid II obtained over conformer 277.

The extreme stabilization of the final product through hydrogen bonding with the free surface silanol has underlined the critical role that the surface silanols played in CO<sub>2</sub> capture over amine-modified solid sorbents and was in total agreement with the previously reported findings [15, 70, 92]. Due to the proximity of the product to the free surface silanol, presence of surface-involved carbamic acid mechanism that was proposed by Cho et al. [15] was also investigated, but no such reaction pathway could be identified over conformer 277.

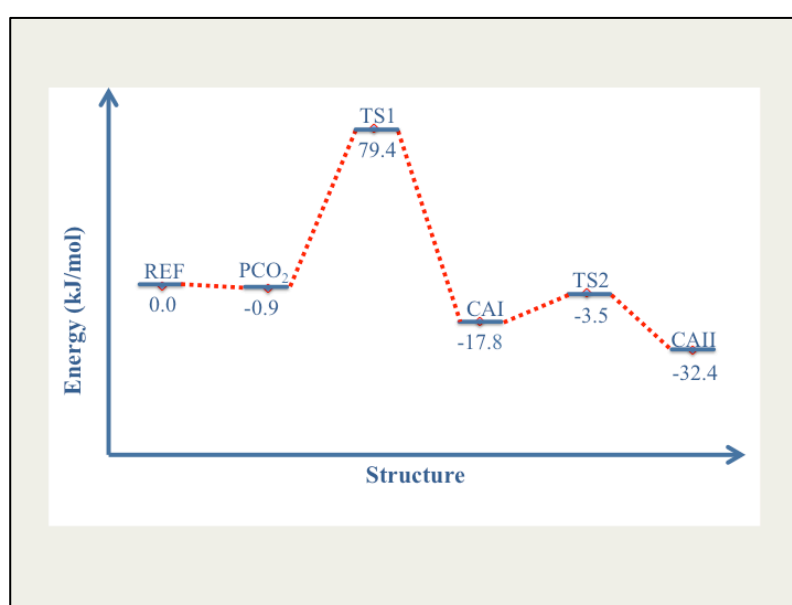


Figure 4.14. Reaction energy diagram of CO<sub>2</sub> adsorption over conformer 277.

#### 4.1.6. Conformer 30

Conformer 30 (Figure 4.15A) was 5.6 kJ/mol less stable with respect to the lowest-energy conformer. Similar to the previous cases, amine groups were in interaction with each other leaving only  $N_1$  available for  $CO_2$  adsorption.

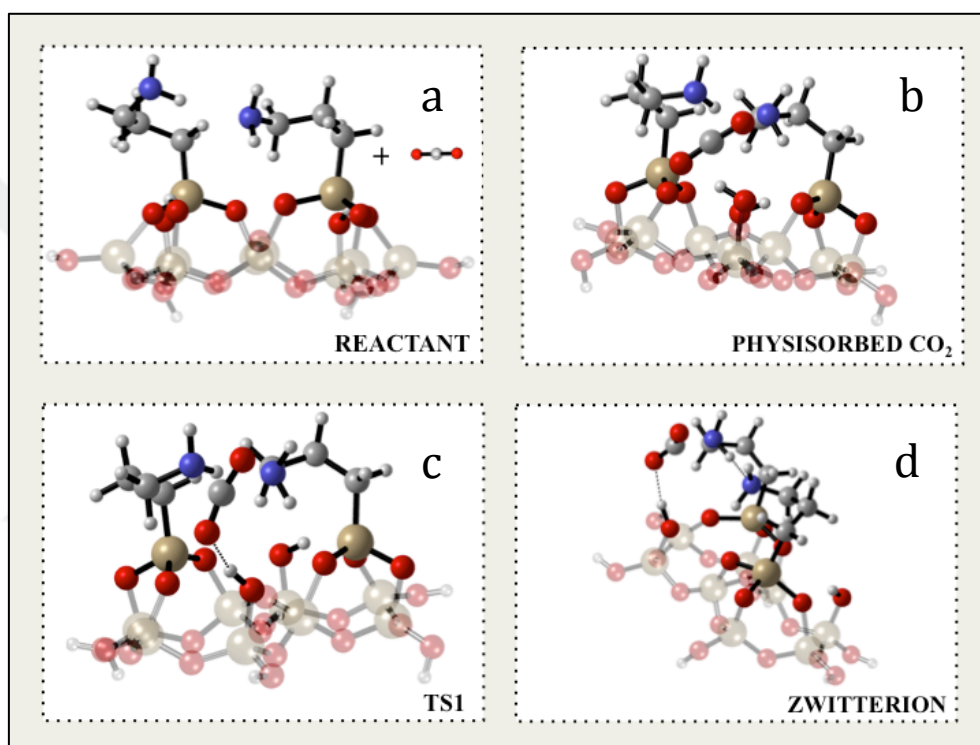


Figure 4.15. Molecular structures of (a) Model 30+ $CO_2$ , (b) Physisorbed  $CO_2$ , (c) Transition state 1, (d) Zwitterionic intermediate.

Adsorption free energy of  $CO_2$  over site  $N_1$  was estimated to be 6.9 kJ/mol. Different from the previous models, physisorbed carbon dioxide (Figure 4.15B) was converted into a zwitterionic intermediate (Figure 4.15D) with an activation energy of 23.2 kJ/mol, zwitterion being stabilized through hydrogen bonding interactions between the -CO of the zwitterion and the free surface silanol and between the -NH of the zwitterion amine and the N of the neighboring amine. Nevertheless, zwitterionic intermediate formation was thermodynamically infeasible with a relative energy of 21 kJ/mol in comparison with the reference state (APTMS-MCM-41+ $CO_2$ ). Zwitterion was subsequently transformed into an

ammonium carbamate structure (Figure 4.16B) through the deprotonation by the neighboring amine (activation energy was 26.8 kJ/mol), which indicated that the observation of the zwitterionic intermediate decreased the activation barrier of carbamate formation significantly. Regardless of the interplay observed between the carbamate, surface silanol and the neighboring amine (surface silanol was hydrogen bonded to the -CO of the carbamate, one of the -NH groups of the ammonium ion was hydrogen bonded to the =CO of the carbamate and another -NH of the ammonium ion was hydrogen bonded to the N of the neighboring amine), carbamate was found to be 49 kJ/mol less stable relative to the reference structure.

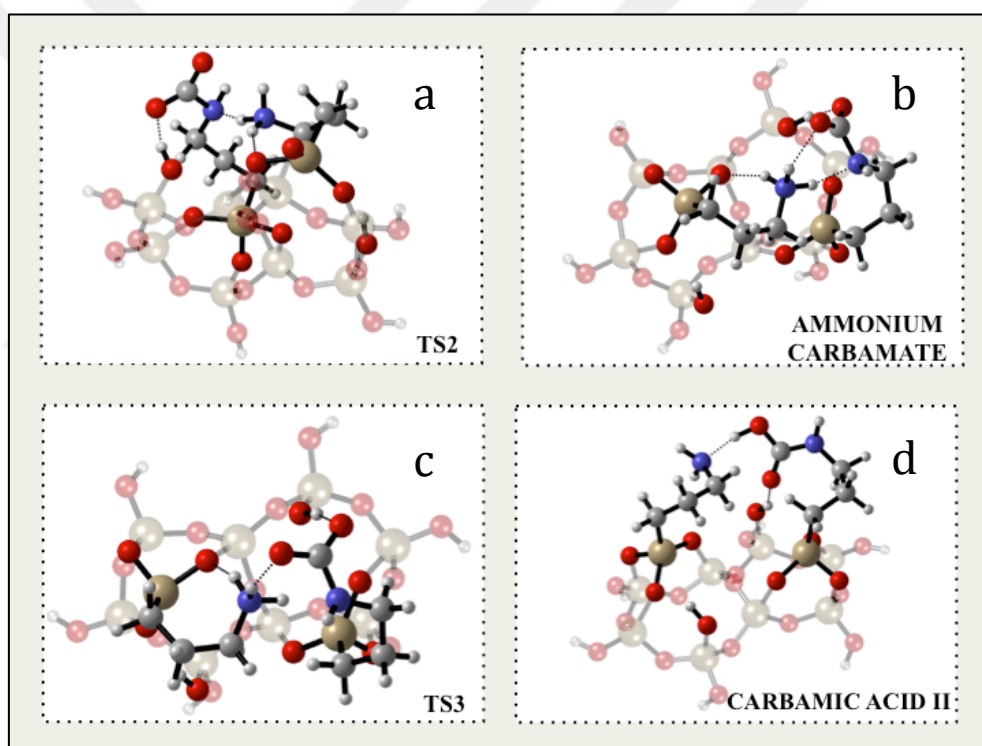


Figure 4.16. Molecular structures of (a) Transition state 2, (b) Ammonium carbamate, (c) Transition state 3, (d) Carbamic acid II.

As it was the case for conformer 720, this carbamate was immediately protonated back by the ammonium ion (activation energy was calculated as 3.3 kJ/mol) leading to the formation of a carbamic acid (Figure 4.16D) with a relative energy of -19.2 kJ/mol with respect to the reference point. Unlike the carbamic acid obtained from carbamate in case of conformer 720, the carbamic acid here was of type II, involving hydrogen bonding

interactions between the -COH of the acid and the -NH of the neighboring amine as well as the =CO of the acid and the -OH of the surface. Due to the proximity of the hydrogens of the neighboring amine, this carbamic acid was then observed to be transformed into another carbamic acid structure (Figure 4.15B) through the simultaneous transfer of the carbamic acid proton to the neighboring amine and another proton of the neighboring amine to the -CO group of the acid. Activation energy regarding this conversion was calculated to be 29.2 kJ/mol; the resulting structure was hydrogen bonded to the neighboring amine only through the -COH group indicating that it was of type I. Due to the reduced interactions with the surface silanols and the neighboring amine, the second carbamic acid was 4 kJ/mol less stable than the first one. Still, it had a relative energy of -15.2 kJ/mol with respect to the reference structure meaning that both carbamic acids may be observed in the product stream. Reaction energy diagram regarding the explained mechanism is presented in Figure 4.16.

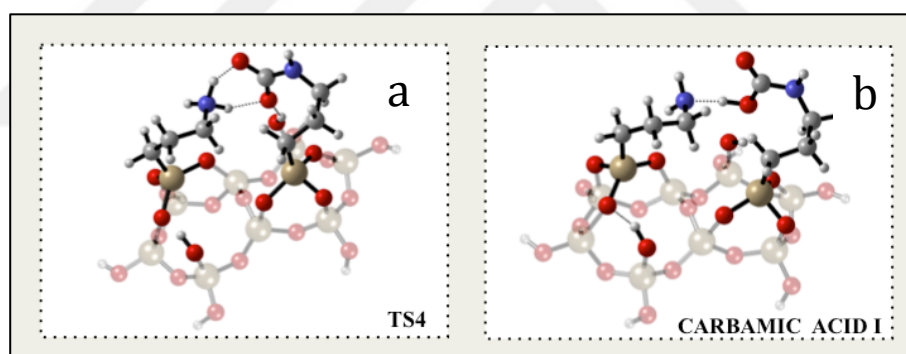


Figure 4.17. Molecular structures of (a) Transition state 4, (b) Carbamic Acid I of reaction pathway I.

Due to the proximity of the surface silanol to the type II carbamic acid observed in the reaction pathway, surface-involved carbamic acid formation (previously proposed by Cho et al. [15]) was also investigated and an alternative pathway in which the surface silanol played an active role in the proton transfer was identified. According to the observed pathway (Figure 4.18), upon the formation of type II carbamic acid (through the protonation of the carbamate by the ammonium), a simultaneous proton transfer from the -COH of acid to the neighboring amine and from the surface silanol to the =CO of the acid



took place resulting in the formation of a carbamic acid-ammonium-surface siloxide complex (Figure 4.17B) with an energy of 34.6 kJ/mol relative to the reference point.

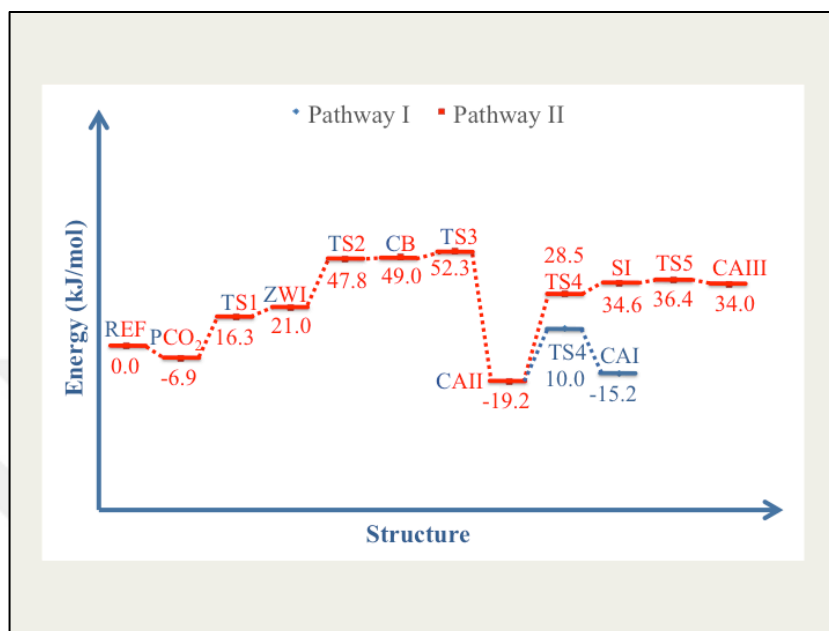


Figure 4.18. Reaction energy diagram of CO<sub>2</sub> adsorption over conformer 30.

Proton-deficient surface siloxide was then protonated by the ammonium ion producing another carbamic acid that was hydrogen bonded to the surface silanol through -COH and to the neighboring amine through =CO. This species was denoted as type III carbamic acid (Figure 20). Activation barriers required for the two steps were calculated to be 47.7 kJ/mol and 1.8 kJ/mol, respectively. Final product was, however, 34 kJ/mol less stable relative to the reference state implying the thermodynamic infeasibility of the reaction pathway of interest. Schematic representation of the surface-involved mechanism is presented in Figure 4.19 as Pathway II.

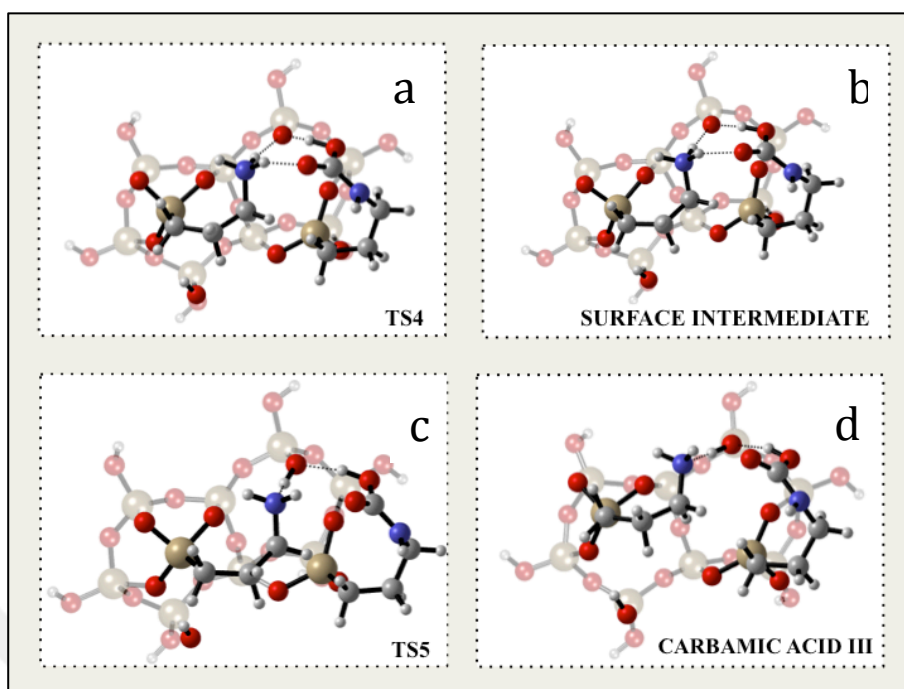


Figure 4.19. Molecular structures of (a) Transition state 4, (b) Surface intermediate, (c) Transition state 5, (d) Carbamic acid III of reaction pathway II.

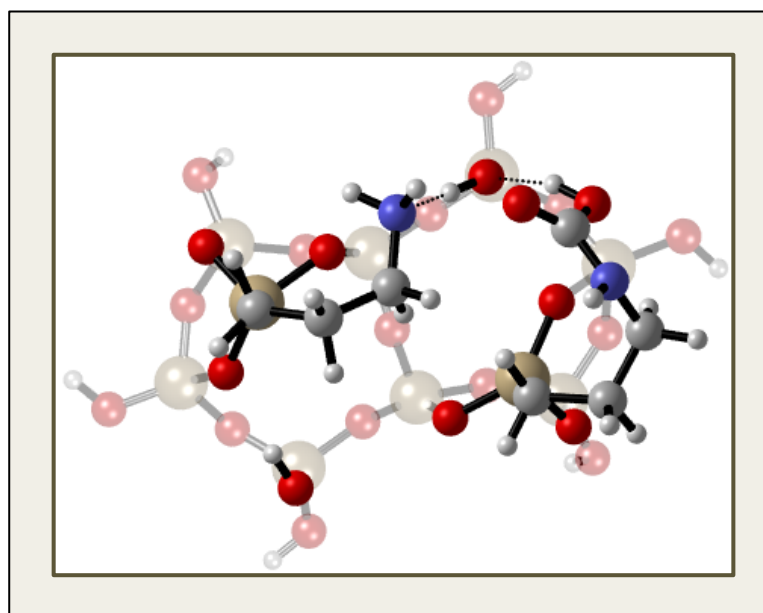


Figure 4.20. Molecular Structures of Type-III Carbamic Acid

#### 4.1.7. General Considerations

Although early findings on CO<sub>2</sub> adsorption over APTMS-modified mesoporous silica reported the formation of carbamic acid as an intermediate to the carbamate production or as the final product when the neighboring amines are absent [16, 71, 73, 93], identification of various carbamic acid structures differing from one another in their stabilities and the hydrogen bonding network that they are involved in has changed this belief considerably [14, 15, 74]. Our calculations demonstrating that carbamic acids of types I and II were the two main adsorption products obtained for CO<sub>2</sub> adsorption over model 5\_5 were, in this manner, parallel to the much recent findings [14]. The molecular structure of the type II carbamic acid was indeed almost identical to the structure proposed for the frequently observed <sup>13</sup>C resonance at 164.3 ppm [14, 73, 74], while type I carbamic acid was reported for the first time in this study.

Type II carbamic acid was found to be more stable than type I owing to the increased hydrogen bonding interactions observed in the former due to the involvement of surface silanol. In addition to stabilizing the intermediates and products, surface silanols were shown to play an active role in the reaction mechanism of CO<sub>2</sub> capture (for model 30) in agreement with the previous findings [15]. According to this previously reported reaction mechanism, CO<sub>2</sub> was weakly adsorbed over one of the nitrogen sites available with an adsorption energy of 23.9 kJ/mol in terms of electronic energy. This weakly adsorbed CO<sub>2</sub> adsorption complex was next converted into a zwitterion-ammonium-siloxide complex (-31.8 kJ/mol relative to the reference point) through a proton transfer from the surface silanol to the neighboring amine that was followed by the proton migration from the nearby silanol to the siloxide forming an intermediate made of another zwitterion-ammonium-siloxide complex (-15.9 kJ/mol relative to the reference). Activation barriers required for these two steps were recorded as 31.8 kJ/mol and 25 kJ/mol, respectively. This complex was then transformed into an ammonium carbamate (-81.2 kJ/mol relative to the reference) that was hydrogen bonded to two surface silanols through its -CO group subsequent to the deprotonation of the zwitterion by the adjacent siloxide with an activation barrier of 33.9 kJ/mol. Finally, this surface-stabilized carbamate was converted into a surface-involved carbamic acid through the protonation of carbamate by the surface silanol. Activation energy of this step was reported to be 2.5 kJ/mol whereas the final

product had an energy of -80.8 kJ/mol relative to the reference state [15]. A direct carbamic acid (-64.4 kJ/mol) formation pathway was also presented with a reaction barrier of 58.1 kJ/mol indicating that the reaction was more facile when surface silanols were involved in the protonation/deprotonation [15]. As may be remembered from the discussions of model 30, however, surface-involved mechanism was in our case less favorable than the conventional carbamic acid production mechanism where the transition states, intermediates and products were stabilized by hydrogen bonding interactions with the neighboring amine and surface silanol. Although our findings seemed to contradict to that of Cho et al. at first sight, it should be noted that they computed the direct carbamic acid formation path (which led to a type I carbamic acid) in the absence of the SiO<sub>2</sub> surface by freezing the two terminal carbon atoms at an intermolecular distance of 6Å to mimic the immobilization of the APTMS structures through grafting [15]. However, our calculations demonstrated that the presence of the silica surface had a critical role on the reaction mechanism, energetics and surface stabilities of the reaction products and intermediates. Hence, their comparison of the two reported mechanisms (direct carbamic acid formation and surface-involved) and conclusion that surface-involved mechanism was more feasible does not make sense, indeed. Besides, the energy values reported in the study of Cho et al. were electronic energies. Relative electronic energies of type I carbamic acid structures computed in this study with respect to the reference states ranged from -44.2 kJ/mol to -66.8 kJ/mol being in perfect agreement with that of Cho et al. [15].

#### **4.2. REACTION PATHWAY ANALYSIS OVER MODEL 5\_4\_5**

The second model had a surface density of 3.40 molecules/nm<sup>2</sup> and four free surface silanols available after modification. Considering the surface amine densities achieved in experimental studies [44], model 5\_4\_5 may still be regarded as a high-density model.

As it was mentioned in the previous section, 3 different conformers –namely 254, 287 and 473– were considered for reaction pathway analysis. Due to the larger surface area of the selected model, APTMS molecules were more packed onto the silica surface which would result in more interactions with the surface silanols.

#### 4.2.1. Conformer 254

254 (Figure 4.18A) was the lowest-energy conformer of the model 5\_4\_5 over which CO<sub>2</sub> adsorption was possible. Stabilization of the model was achieved through the interaction of the APTMS molecule (the one that was much closer to the surface) with the neighboring amine as well as the two surface silanols located crosswise at the two sides of the cluster. Due to the interaction of the two amines, lone pair on N<sub>2</sub> was occupied leaving N<sub>1</sub> as the only CO<sub>2</sub> adsorption site.

Three different reaction mechanisms were identified for CO<sub>2</sub> adsorption over conformer 254, two of them being surface-involved mechanisms. According to the conventional pathway in which the surface silanols do not participate directly, CO<sub>2</sub> was found to adsorb weakly on site N<sub>1</sub> with an adsorption energy of 0.69 kJ/mol. This adsorption complex was next converted into a zwitterionic intermediate (22 kJ/mol less stable than the reference state) that was hydrogen bonded to one of the surface silanols present at the surface. Reaction barrier calculated for this step was 20.5 kJ/mol. Similar to what have been observed for conformer 30 in the previous section, zwitterion (Figure 4.18D) was subsequently transformed into a carbamate (Figure 4.19B) and carbamate into a carbamic acid (figure 4.19D). Carbamate formation required an activation energy of 12.3 kJ/mol, while the conversion of carbamate to carbamic acid was spontaneous with a barrier of -4.0 kJ/mol. Although the activation barrier for zwitterion formation over conformer 254 was comparable to that of the conformer 30 of the previous section, the next two activation energies were significantly lower in the presence of more surface silanols. Besides, carbamate had a relative energy of -30.9 kJ/mol with respect to the reference state (APTMS-MCM-41+CO<sub>2</sub>), the stability being originated from the complex hydrogen bonding network occurring between the =CO of the carbamate and surface silanol, =CO of the carbamate and -NH of ammonium, -CO of the carbamate and the surface silanol, -CO of the carbamate and the -NH of ammonium. The structure of the carbamate observed here did not resemble the previously reported structures [15, 16, 74].

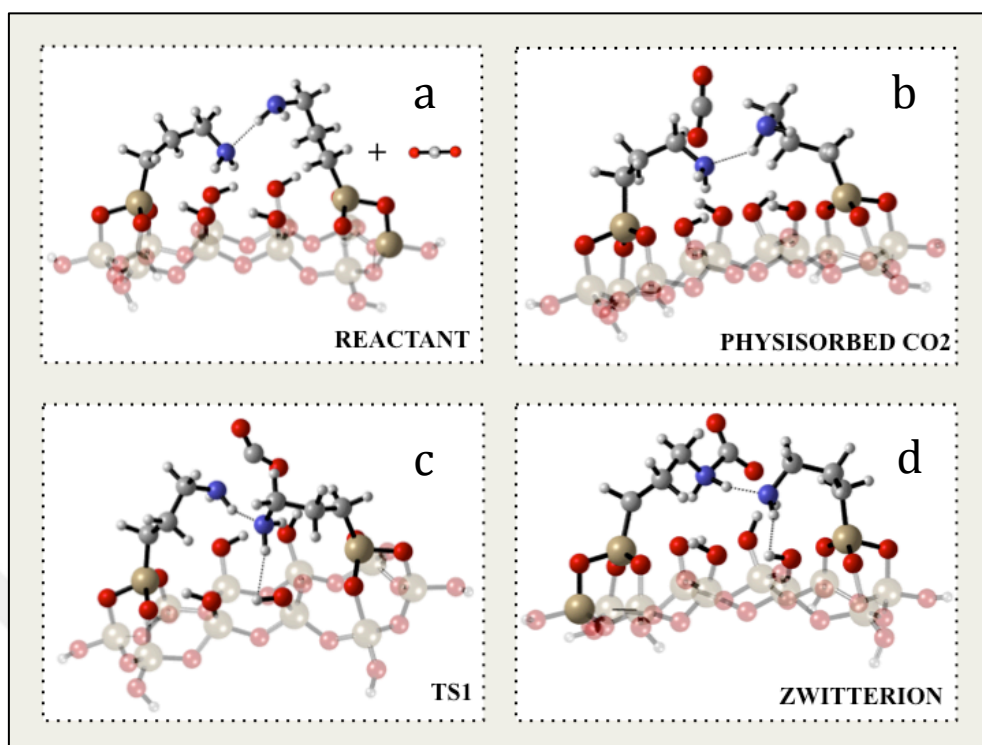


Figure 4.21. Molecular structures of (a) Model 254+CO<sub>2</sub>, (b) Physisorbed CO<sub>2</sub>, (c) Transition state 1, (d) Zwitterionic intermediate.

Carbamic acid, which was obtained through the protonation of the carbamate, was estimated to be 38.5 kJ/mol more stable relative to the reference state. This carbamic acid was of type II, involving two hydrogen bonding interactions with the surface silanol and the neighboring amine through the =CO and -COH groups, respectively. The structures of the intermediates, transition states and products are given in Figure 4.21 and 4.22, while the reaction mechanism is depicted in Figure 4.23.

According to the second pathway observed, –instead of being converted into a carbamate–zwitterion acquired a proton from the nearby surface silanol, and the proton deficient silanol from another nearby silanol producing an intermediate structure involving a surface siloxide and -NH<sub>2</sub>COOH (Figure 4.24B) with an activation energy of 43.8 kJ/mol.

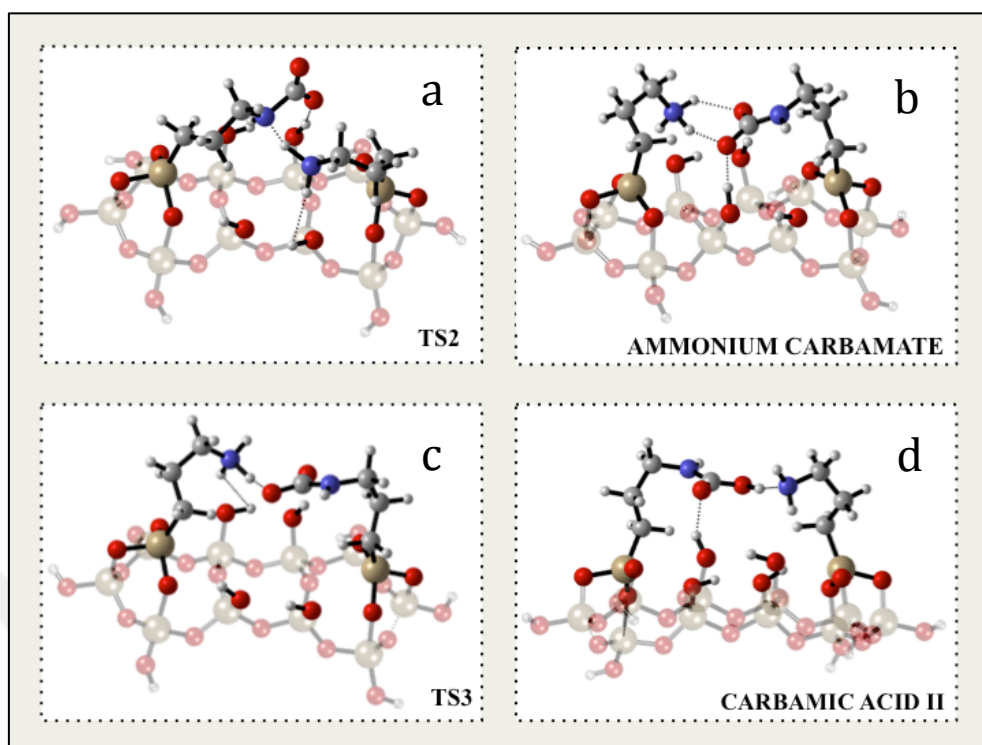


Figure 4.22. Molecular structures of (a) Transition state 2, (b) Ammonium carbamate, (c) Transition state 3, (d) Carbamic acid II of reaction pathway I.

Following this, siloxide was protonated by the  $\text{-NH}_2\text{COOH}$  structure (with a barrier of 0.8 kJ/mol) producing a type I carbamic acid (Figure 4.24D) that was hydrogen bonded only through its  $\text{-COH}$  group. Being a type I carbamic acid, this structure was 27.5 kJ/mol less stable in comparison with the reference state.

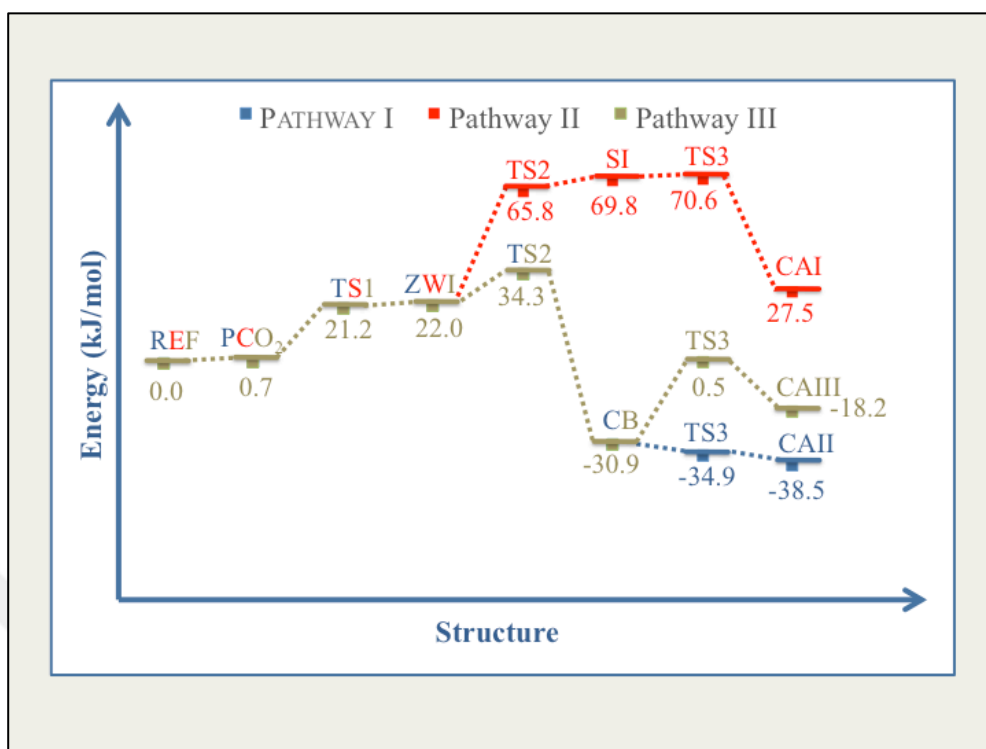


Figure 4.23. Reaction energy diagram of CO<sub>2</sub> adsorption over conformer 254.

Similar to the conformer 30 of the previous section, surface-involved reaction mechanism was much less favorable with respect to the conventional mechanism discussed above. Reaction energy diagram is presented in Figures 4.23 whereas the intermediates, transition states and products are given in Figures 4.24.



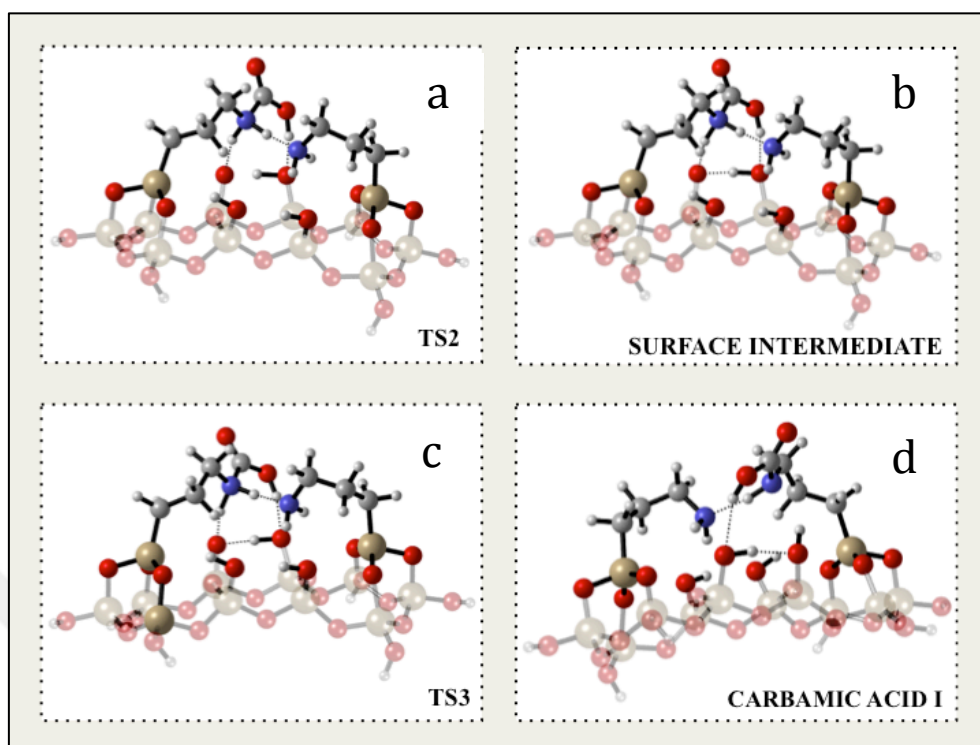


Figure 4.24. Molecular structures of (a) Transition state 2, (b) Surface intermediate, (c) Transition state 3, (d) Carbamic acid I of reaction pathway II.

According to the third mechanism, on the other hand, carbamate structure (Figure 4.21B) was converted into a type III carbamic acid (Figure 4.25B) that was involved in two hydrogen bonding between the surface silanol and the neighboring amine through its -COH and =CO groups, respectively. This conversion was accompanied by a simultaneous proton transfer from one of the surface silanols to the carbamate, from a nearby silanol to this siloxide and from the ammonium to the second siloxide formed. This step required an activation barrier of 31.4 kJ/mol; type III carbamic acid obtained in the end was 18.2 kJ/mol more stable relative to the reference state and contrary to what was reported by Cho et al. [15], surface-involved mechanisms were less feasible than the conventional pathways and the siloxide-involving structures were not stable. Reaction pathway is presented in Figure 4.23 and the species observed along the reaction pathway are given in Figure 4.25.

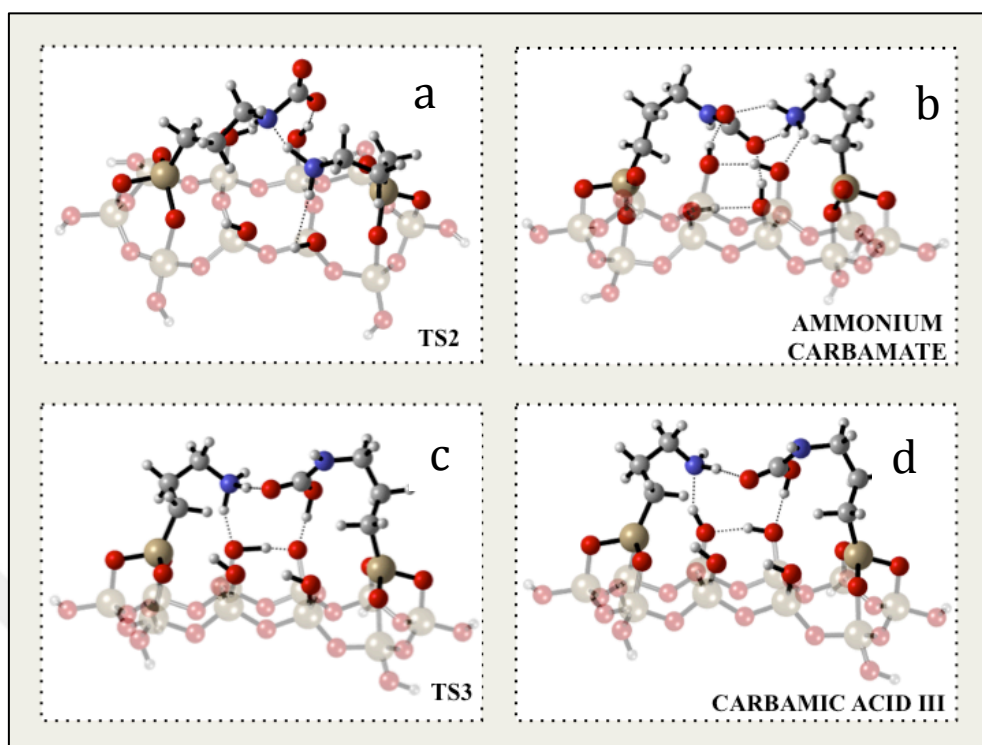


Figure 4.25. Molecular structures of (a) Transition state 3, (b) Carbamic acid III of reaction pathway III. , (c) Transition state 3, (d) Carbamic acid III of reaction pathway III.

#### 4.2.2. Conformer 287

Conformer 287 (Figure 4.26A) was 4.8 kJ/mol less stable compared to the lowest-energy conformer 254. Due to the proximity of the APTMS molecules to the surface and to each other, they were in interaction with each other and the surface which in turn stabilized the structure. Site  $N_2$  was more available for  $CO_2$  capture and the adsorption energy was calculated as 13.1 kJ/mol over  $N_2$ .

Similar to conformer 254, three distinct reaction pathways were identified for  $CO_2$  adsorption, two of them being surface-involved mechanisms. According to the first of them, where the surface silanols did not take part directly, physisorbed carbon dioxide (Figure 4.26B) was converted into a silanol-stabilized zwitterionic intermediate (Figure 4.26D) with an activation energy of 9.5 kJ/mol. Zwitterion, which possessed a relative energy of 1.1 kJ/mol with respect to the reference state (APTMS-MCM-41+ $CO_2$ ), was next

transformed into an ammonium carbamate ion pair (Figure 4.27B) that was significantly less stable than the carbamate structure observed for conformer 254. Reduced stability of the conformer (3.97 kJ/mol relative to the reference state) was originating from the diminished hydrogen bonding interactions, carbamate was now hydrogen bonded to one of the surface silanols and the neighboring amine through its =CO and -CO groups, respectively.

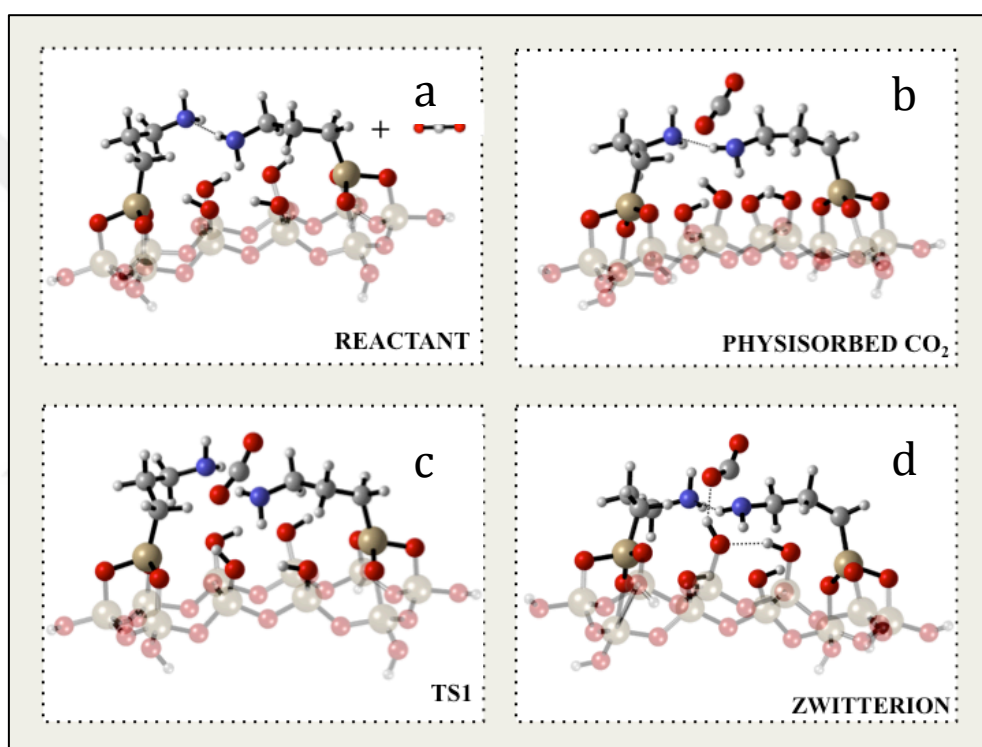


Figure 4.26. Molecular structures of (a) Model 287+CO<sub>2</sub>, (b) Physisorbed CO<sub>2</sub>, (c) Transition state 1, (d) Zwitterionic intermediate.

Estimated activation barrier for this step was 27.3 kJ/mol. Once the carbamate was formed, it was protonated back by another proton of the ammonium to form a carbamic acid (Figure 4.27D) spontaneously with a relative energy of -4.5 kJ/mol. Resulting structure interacted with the neighboring amine and the surface silanol through -COH and =CO, respectively; so it was of type II. Despite of being a type II carbamic acid, however, it was found to be significantly less stable compared to the type II carbamic acid obtained over conformer 254. Our calculated relative energy for carbamic acid of conformer 287 (-4.5

kJ/mol) indeed agreed very well with the reported values (-5.6 kJ/mol) of Mafra et al. [4], which in turn implied that the actual structures of the three commonly observed  $^{13}\text{C}$  resonances might be quite different than the ones suggested by various groups [32 of 6, 6, 5]. Molecular structures of the reactants, transition states and products of the reaction pathway I are presented in Figures 4.26 and 4.27 while the reaction energy diagram may be found in Figure 4.28.

The remaining two reaction pathways involve the conversion of the zwitterionic intermediate into carbamic acid by direct commitment of the surface silanols in the proton transfer, the difference being the number of silanols being engaged in the reaction mechanism.

Accordingly, carbamic acid (Figure 4.29 B) formation took place through the simultaneous transfer of protons from a surface silanol to the =CO of the zwitterion and from the  $-\text{NH}_2$  of the zwitterion to the siloxide formed upon zwitterion protonation in the second mechanism (Figure 4.28). The resulting carbamic acid (36.4 kJ/mol relative to the reference state) belonged to none of the three classes defined before and comprised hydrogen bonding interactions between the  $-\text{NH}$  of the carbamic acid and the neighboring amine; between the N of the carbamic acid and the surface  $-\text{OH}$ .

The third mechanism (Figure 4.28), on the other hand, achieved the zwitterion conversion into a carbamic acid (47.6 kJ/mol relative to the reference state) via a simultaneous proton transfer from the surface silanol to =CO of the zwitterion, from the neighboring silanol to siloxide, and from the  $-\text{NH}_2$  of the zwitterion and the siloxide.

A similar hydrogen bonding network to that of the second mechanism occurred in the obtained structure (Figure 4.30B), keeping it out of the classification made before. Based on the high activation barriers ( $\sim 76$  kJ/mol and  $\sim 60$  kJ/mol, respectively) and low carbamic acid stabilities of the second and third mechanisms, it was obvious that surface-involved carbamic acid formation was unfavorable with respect to the conventional pathway. The reaction energy diagram of all three mechanisms of the conformer 287 are depicted in Figure 4.28.

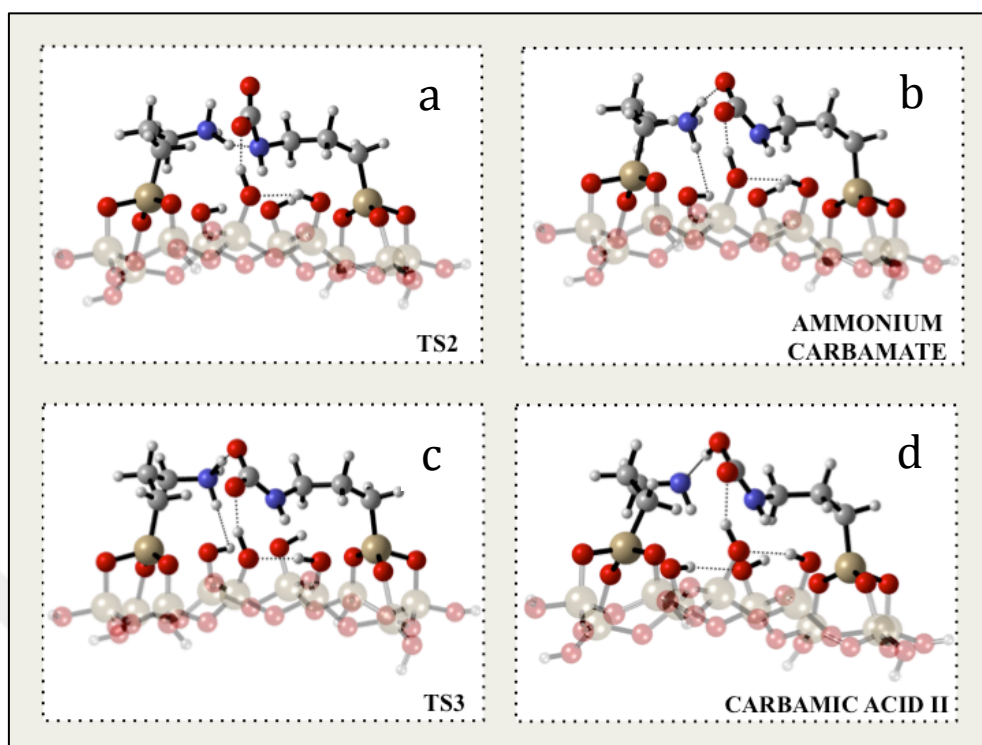


Figure 4.27. Molecular structures of (a) Transition state 2, (b) Ammonium carbamate, (c) Transition state 3, (d) Carbamic acid II of reaction pathway I.

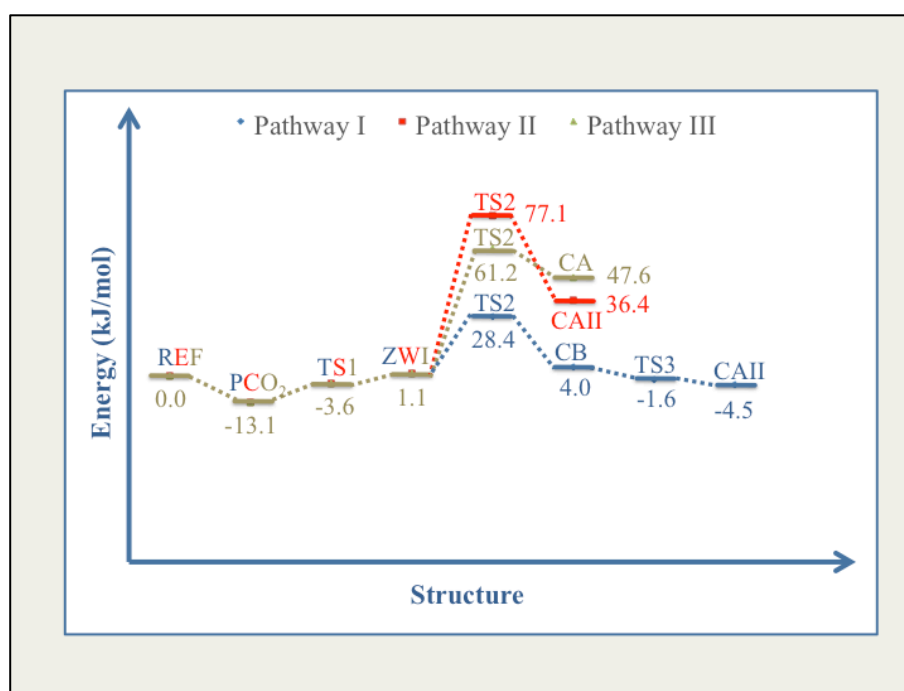


Figure 4.28. Reaction energy diagram of CO<sub>2</sub> adsorption over conformer 287.

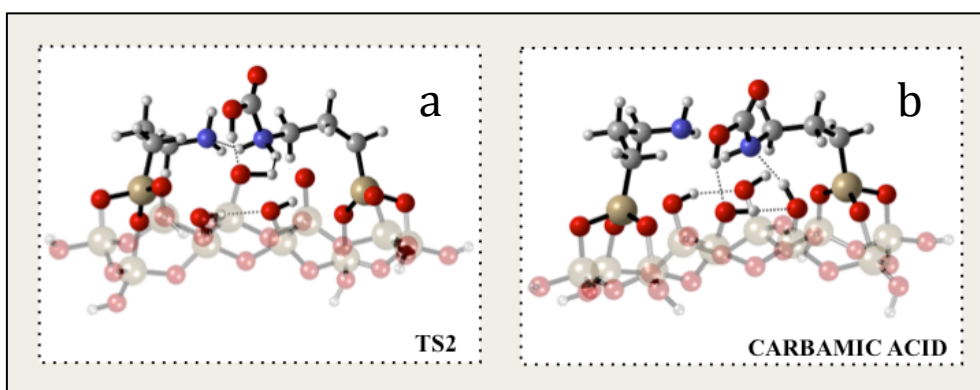


Figure 4.29. Molecular structures of (a) Transition state 2, (b) Carbamic acid of reaction pathway II.

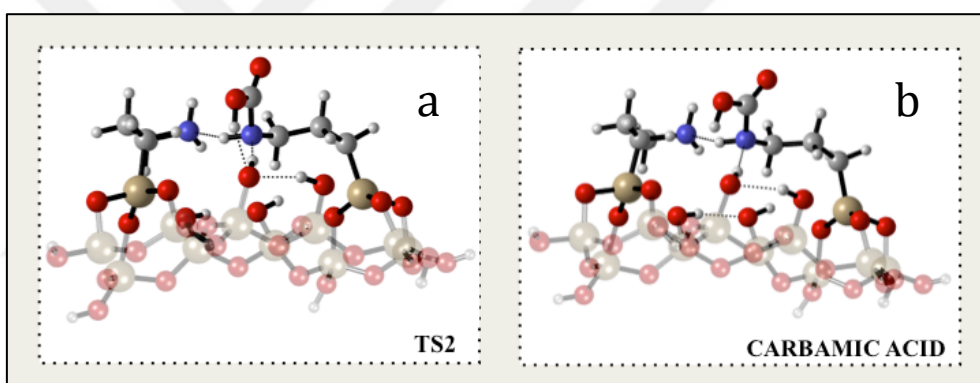


Figure 4.30. Molecular structures of (a) Transition state 2, (b) Carbamic acid of reaction pathway III.

### 4.2.3. Conformer 473

Conformer 473 (Figure 4.31A) was 8.8 kJ/mol less stable than the lowest-energy conformer. The  $N_1$ -H- $N_2$  angle between the two amino groups were bent significantly so that the interaction between them did not occupy the lone pair on any of the nitrogens, making both of them available for  $CO_2$  adsorption.

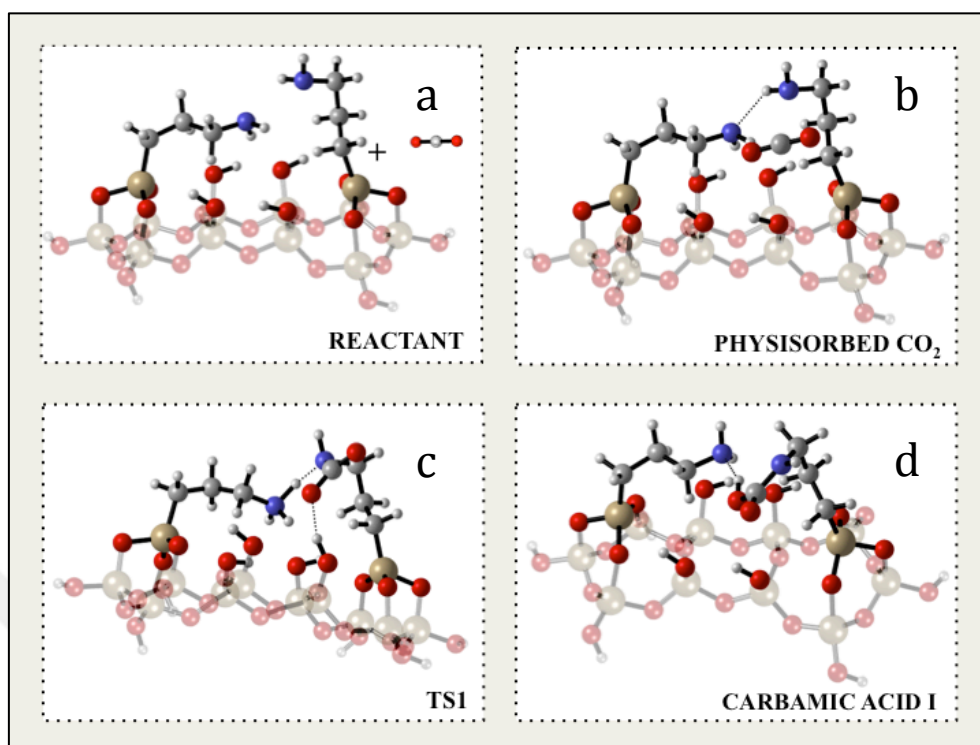


Figure 4.31. Molecular structures of (a) Model 473+CO<sub>2</sub>, (b) Physisorbed CO<sub>2</sub>, (c) Transition state 1, (d) Zwitterionic intermediate over site I.

Adsorption of CO<sub>2</sub> (binding energy being 8.6 kJ/mol) over site 1 resulted in direct carbamic acid formation with an activation energy of 81.3 kJ/mol. The product, being a type I carbamic acid (Figure 4.28D), was hydrogen bonded to the nitrogen of the neighboring amine through its -COH group and had an energy of 24.7 kJ/mol relative to the reference state (APTMS\_MCM-41+CO<sub>2</sub>). Species involved in the corresponding pathway are presented in Figures 4.31, while the schematic representation of the reaction energy diagram may be found in Figure 4.32.

Two distinct pathways were observed for the second site, on the other hand. According to the first one, physisorbed carbon dioxide (Figure 4.33B) (with 5.9 kJ/mol) was converted into a zwitterionic intermediate (Figure 4.33 D) which in turn was transformed into a carbamic acid (Figure 4.35B) through a simultaneous proton transfer from the neighboring amine to the =CO of the zwitterion and from the zwitterion amine to the neighboring one. The resulting carbamic acid was of type II and hydrogen bonded to both the neighboring amine and the surface silanol through its -COH and =CO groups, respectively. Activation

barrier of zwitterion formation was  $\sim 9.0$  kJ/mol, while carbamic acid production required an energy of 36.3 kJ/mol. Relative energies of the zwitterionic intermediate and the type II carbamic acid were calculated as 11.5 and -27.6 kJ/mol, respectively demonstrating that type II carbamic acid was the main product observed over conformer 473. The schematic representation of the reaction energy diagram may be found in Figure 4.34.  $\text{CO}_2$  adsorption species observed along the reaction pathway are given in Figures 4.33 and 4.35.

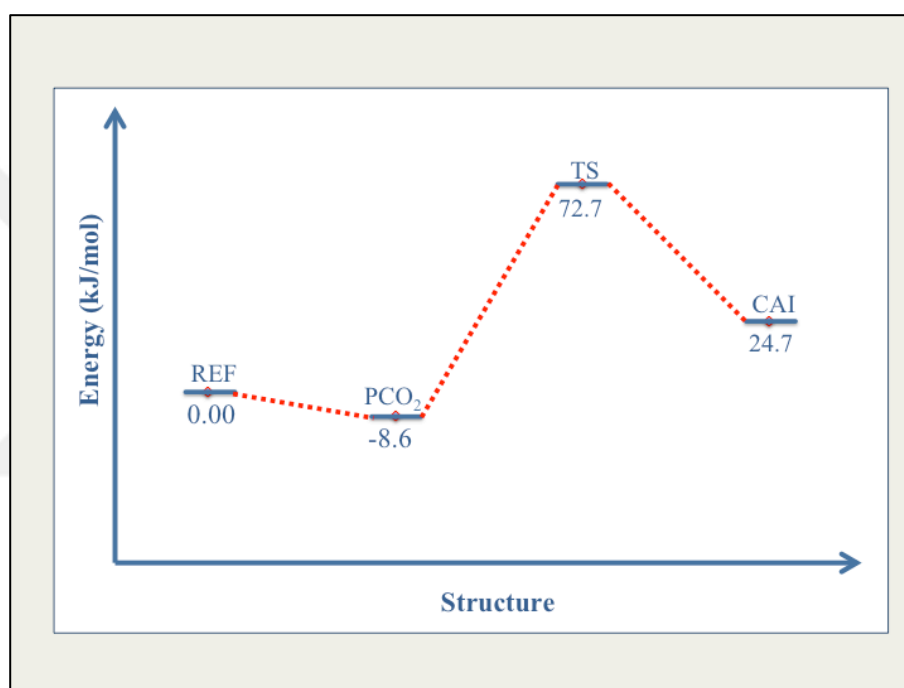


Figure 4.32. Reaction energy diagram of  $\text{CO}_2$  adsorption over conformer 473 (Site I).

The next mechanism identified over conformer 473 was a surface-involved mechanism which contained the conversion of the zwitterion (Figure 4.33D) into another carbamic acid (Figure 4.36B) through a simultaneous proton transfer from one of the surface silanols to the zwitterion, from a nearby silanol to the siloxide and from the amine of the zwitterion to the siloxide.



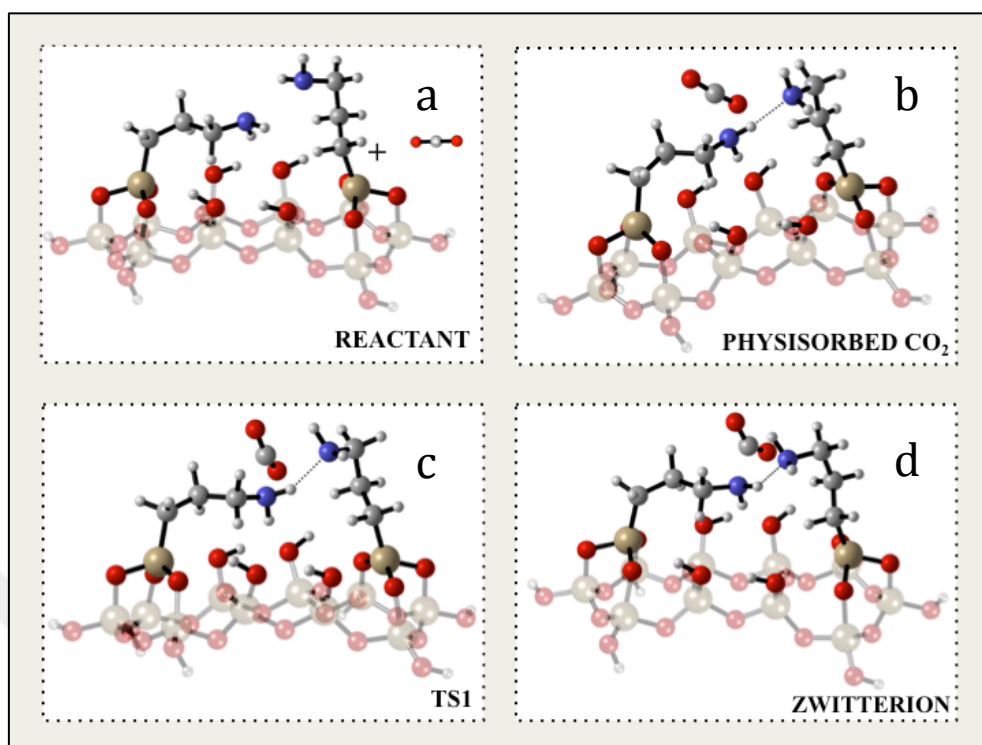


Figure 4.33. Molecular structures of (a) Model 473+CO<sub>2</sub>, (b) Physisorbed CO<sub>2</sub>, (c) Transition state 1, (d) Zwitterionic intermediate over site II.

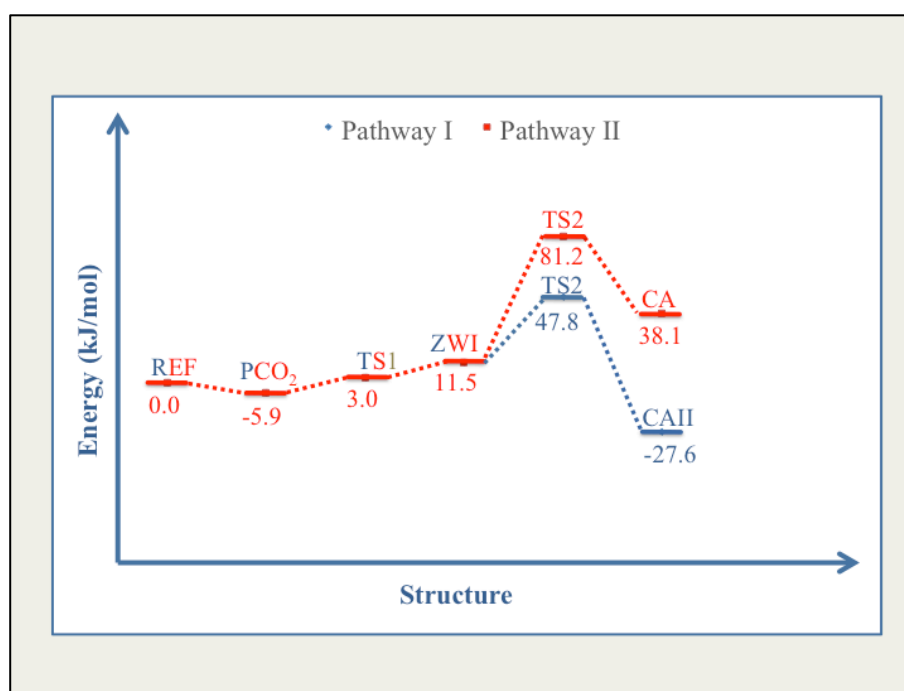


Figure 4.34. Reaction energy diagram of CO<sub>2</sub> adsorption over conformer 473 (Site II).

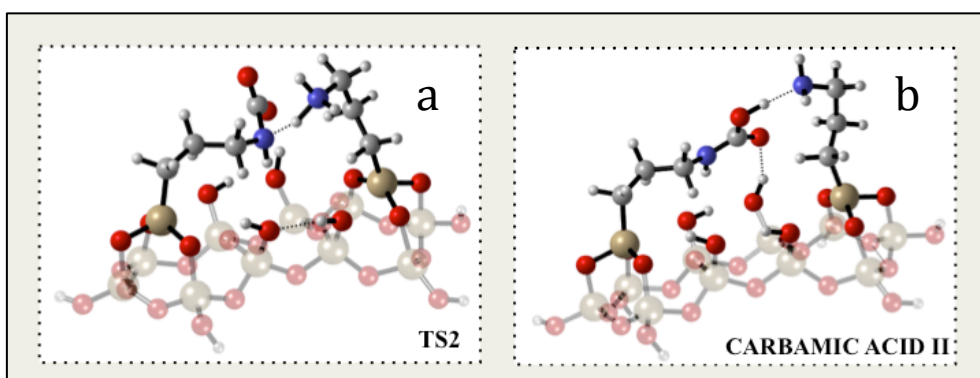


Figure 4.35. Molecular structures of (a) Transition state 2, (b) Carbamic acid II over site II for reaction pathway I.

The activation barrier calculated for this step was 69.7 kJ/mol and the product was involved in hydrogen bonding interactions with the oxygen of the surface silanol and the hydrogen of another surface silanol through its -COH group and nitrogen, respectively. This structure, being quite similar to that obtained through the surface-involved CO<sub>2</sub> adsorption mechanism of conformer 287, did not belong to any of the classes of carbamic acid defined before and had a relative energy of 38.1 kJ/mol with respect to the reference state. Reaction energy diagram of this mechanism is given in Figure 4.34.

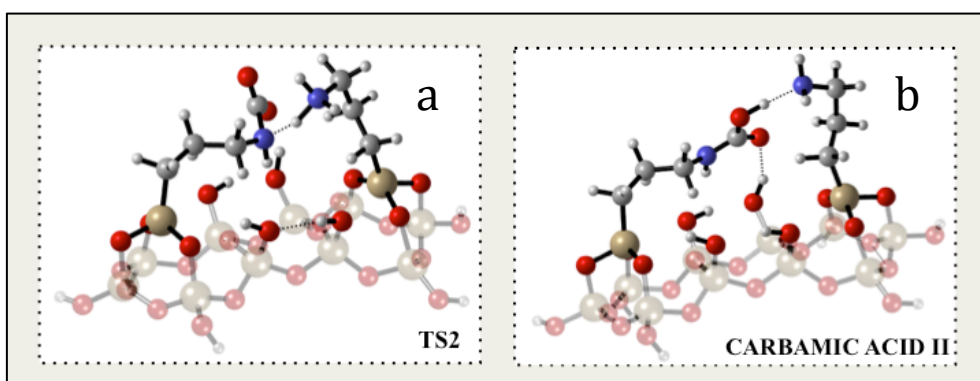


Figure 4.36. Molecular structures of (a) Transition state 2, (b) Carbamic acid over site II for reaction pathway II.

## 5. CONCLUSIONS AND RECOMMENDATIONS

This study objected to investigate the reaction mechanism of CO<sub>2</sub> adsorption over APTMS-modified mesoporous silica sorbent by using DFT modelling. Our calculations, performed by using two clusters of different size and surface amine density, demonstrated that surface silanols played a critical role on the capture of carbon dioxide. Following conclusions maybe driven from the calculations implemented:

- Five distinct pathways, namely direct carbamate formation, direct carbamic acid formation, carbamate conversion to carbamic acid, carbamic acid conversion to another carbamic acid and surface-involved carbamic acid formation, were identified over the models studied.
- Among these, direct carbamate formation and direct carbamic acid formation reactions observed without the existence of the zwitterionic intermediate always took place when the interactions with the surface silanols are restricted. Kinetic barriers calculated for these reaction pathways were much higher and the reaction products generated were always thermodynamically unstable indicating that these two mechanisms were infeasible.
- Stabilization of the zwitterionic intermediate through the hydrogen bonding interactions decreased the required activation barriers and led to the formation of more stable carbamic acid products with respect to the direct formation mechanisms.
- Carbamic acid formation pathway through the conversion of ammonium carbamate was found to be the most favorable mechanism for CO<sub>2</sub> adsorption over APTMS-modified mesoporous silica implying that carbamate was an intermediate structure for the carbamic acid.
- Direct participation of the surface silanols in the reaction mechanism was possible but the surface-involved mechanisms were usually less favorable compared to the carbamic acid formation through carbamate formation. However, interactions with the surface silanols without being involved in the mechanism played a critical role in the stabilization of the reaction species as well as the lessening of the activation barriers.

- Carbamate and carbamic acid were the two main structures of CO<sub>2</sub> adsorption, carbamate being usually less stable than the carbamic acid.
- 3 different types of carbamic acid were identified differing from one another in the hydrogen bonding networks that they were involved in. Type II carbamic acid was usually more stable with respect to the other two types.
- Conversion between the various types of carbamic acid structures was possible.

The following recommendations will be beneficial for the future work with the aim of clarifying the interaction mechanism of CO<sub>2</sub> over amine functionalized mesoporous silica sorbents:

- Aminosilanes involving functionalities other than primary (secondary, tertiary) may be investigated.
- Molecular models with lower surface amine densities (meaning larger mesoporous silica clusters and more silanols at the surface) may be employed.
- Water effect on the reaction mechanism and products may be studied.
- Formation of isolated carbamic acid may be investigated.
- Multi amine-modified mesoporous silica may also be considered in order to study the possibility of intramolecular CO<sub>2</sub> adsorption.

## REFERENCES

1. Adus H. Greenhouse gas mitigation technology: An overview of the CO<sub>2</sub> capture and sequestration studies and further activities of the IEA Greenhouse Gas R&D Programme. *Energy* 22. 1997;22(2-3):217-21.
2. Sayari A, Belmabkhout Y, Serna-Guerrero R. Flue gas treatment via CO<sub>2</sub> adsorption. *Chem. Eng. J.* 2011;171:760-74.
3. Samanta A, Zhao A, Shimizu GKH, Sarkar P, Gupta R. Post-combustion CO<sub>2</sub> capture using solid sorbents: A review. *Ind Eng Chem.* 2012;51:1438-63.
4. Belmabkhout Y, Sayari A. Effect of pore expansion and amine functionalization of mesoporous silica on CO<sub>2</sub> Adsorption over a wide range of conditions. *Adsorption.* 2009;15(3):318-28.
5. Belmabkhout Y, Sayari A. Isothermal versus non-isothermal adsorption-desorption cycling of triamine-grafted pore-expanded MCM-41 mesoporous silica for CO<sub>2</sub> capture from flue gas. *Energy Fuel.* 2010;24(9):5273-80.
6. Srivatsa SC, Bhattacharya S. Amine-based CO<sub>2</sub> capture sorbents: a potential CO<sub>2</sub> hydrogenation catalyst. *J. Co2 Util.* 2018;26:397-407.
7. Meng Y, Jiang J.G, Gao YC, Yan F, Liu N, Aihemaiti A. Comprehensive study of CO<sub>2</sub> capture performance under a wide temperature range using poly-ethyleneimine-modified adsorbents. *Journal of CO2 Utilization.* 2018;27:89-98.
8. Chang FY, Chao KJ, Cheng HH, Tan C.S. Adsorption of CO<sub>2</sub> onto amine-grafted mesoporous silicas. *Sep. Purif. Technol.* 2009;70(1):87-95.
9. Hiyoshi N, Yogo K, Yashima T. Adsorption characteristics of carbon dioxide onorganically functionalized SBA-15. *Microporous and Mesoporous Materials* 2005;84:357-65.
10. Kishor R, Ghoshal AK. Amine-modified mesoporous silica for CO<sub>2</sub> adsorption: the role of structural parameters. *Int. Eng. Chem. Res.* 2017;56(20):6078-87.

11. Sayari A, Belmabkhout Y., Da'na E. CO<sub>2</sub> deactivation of supported amines: does the nature of matter? *Langmuir*. 2012;28(9):4241-7.
12. Sanz R, Calleja G, Arencibia A, Sans-Perez ES. Amino functionmesostructured SBA-15 silica for CO<sub>2</sub> capture: exploring the relation between the adsorption capacity and the distribution of amino groups by TEM. *Microporous Mesoporous Mater*. 2012;158:309-17.
13. Caplow M. Kinetics of carbamate formation and breakdown. *Journal of Chemical Society*. 1968;24:6795-803.
14. Mafra L, Cendak T, Schneider S, Wiper PV, Pires J, Gomes JRB, Pinto ML. The structure of chemisorbed CO<sub>2</sub> species in amine-functionalized mesoporous silicas studied by solid-state NMR and computer modeling. *J. Am. Chem. Soc*. 2016;139(1):389-408.
15. Cho M, Park JT, Yavuz C, Jung Y. A catalytic role of surface silanol groups in CO<sub>2</sub> capture on the amine-anchored silica support. *Phys Chem Chem Phys*. 2018;20:12149-56.
16. Hahn MW, Jelic J, Berger E, Reuter K, Jentys A, Lercher JA. Role of amine functionality for CO<sub>2</sub> chemisorption on silica. *J. Phys. Chem. B*. 2016;120:1988-95.
17. Working Group III. Climate change 2014: mitigation of climate change. Cambridge University Press., *2014 IPCC 5th Assesment Report of the Intergovermental Panel on climate change*; 2014 : IPCC.
18. CO<sub>2</sub> emissions from fuel combustion, *2016 IEA International Energy Agency* ; 2016 : IEA.
19. Dincer I. *Comprehensive energy systems*. Oxford: Elsevier; 2018.
20. Favre E. Membrane processes and postcombustion carbon dioxide capture: challenges and prospects. *Chem Eng J*. 2011;171:782-93.
21. Working Group III. IPCC special report on carbon dioxide capture and storage. Cambridge University Press., *2005 IPCC Intergovermental Panel on Climate Change*; 2005:IPCC.

22. Tontiwachwuthikul P, Meisen A, Lim CJ. Solubility of CO<sub>2</sub> in 2-amino-2-methyl-1-propanol solutions. *J Chem Eng Data*. 1991;36:130–3.
23. Park SH, Lee KB, Hyun J.C, Kim SH. Correlation and prediction of the solubility of carbon dioxide in aqueous alkanolamine and mixed alkanolamine solutions. *Ind. Eng. Chem. Res.* 2002;41:1658–65.
24. Yih SM, Shen KP. Kinetics of carbon dioxide reaction with sterically hindered 2-amino-2-methyl-1-propanol aqueous solutions. *Ind. Eng. Chem. Res.* 1988;27:2237-41.
25. Alper E. Reaction Mechanism and kinetics of aqueous solutions of 2-amino-2-methyl-1-propanol and carbon dioxide. *Ind. Eng. Chem. Res.* 1990;29:1725-8.
26. Shen KP, Li MH. Solubility of carbon dioxide on aqueous mixtures of monoethanolamine with methyldiethanolamine. *J Chem Eng Data*. 1992;37:96-100.
27. Dawodu OF, Meisen A. Solubility of carbondioxide in aqueous mixtures of alkanolamines. *J Chem Eng Data*. 1994;39:548-52.
28. Li MH, Chang BC. Solubilities of carbondioxide in water+monoethanolamine+2-amino-2-methyl-1-propanol. *J Chem Eng Data*. 1994;39:448-52.
29. Freeman SA, Dugas R, van Wagener DH, Nguyen T, Rochelle GT. Carbon dioxide capture with concentrated, aqueous piperazine. *Int J Greenhouse Gas Control*. 2010;4:119-24.
30. Xu GW, Zhang CF, Qin SJ, Gao WH, Liu HB. Gas-liquid equilibrium in a CO<sub>2</sub>-MDEA-H<sub>2</sub>O system and the effect of piperazine on it. *Ind. Eng. Chem. Res.* 1998;37:1473-7.
31. Bonenfant D, Mimeault M, Hausler R. Determination of the structural features of distinct amines important for the absorption of CO<sub>2</sub> and regeneration in aqueous solution. *Ind. Eng. Chem. Res.* 2003;42:3179-84.
32. Choi SY, Nam SC, Yoon YI, Park KT, Park SJ. Carbon dioxide absorption into aqueous blends of methyldiethanolamine (MDEA) and alkyl amines containing multiple amino groups. *Ind. Eng. Chem. Res.* 2014;53:14451-61.

33. Kim YE, Moon SJ, Yoon YI *et al.* Heat of absorption and absorption capacity of CO<sub>2</sub> in aqueous solution of amine containing multiple amino groups. *Sep Purif Technol.* 2014;122:112-8.
34. CCS Information Team, Capture Ready How does CCS works? 2008 [cited 2019 26 November]. Available from:  
<http://www.captureready.com/EN/Channels/OverViews/showDetail.asp?ClassID=1>
35. Gray ML, Champagne KJ, Fauth D, Baltrus JP, Pennline H. Performance of immobilized tertiary amine solid sorbents for the capture of carbon dioxide. *Int. J. Greenhouse Gas Control.* 2008;2:3–8.
36. Wang J, Huang L, Yang R, et al. Recent advances in solid sorbents for CO<sub>2</sub> capture and new development trends. *Energy Environ. Sci.* 2014;7:3478–518.
37. Hoffman F, Cornelius M, Morell J, Froeba M. Silica-based mesoporous organic-inorganic hybrid materials. *Angew. Chem. Int. Ed.* 2006;45:3216–51.
38. Rath D, Rana S, Parida KM. Organic amine-functionalized silica-based mesoporous materials: an update of syntheses and catalytic applications. *RSC Adv.* 2014;4;57111-124.
39. Franchi RS, Harlick PJE, Sayari A. Applications of pore-expanded mesoporous silica. 2. Development of a high-capacity, water-tolerant adsorbent for CO<sub>2</sub>. *Ind. Eng. Chem. Res.* 2005;44(21):8007-13.
40. Doadrio AL, Salinas AJ, Montero JMS, Regi MV. Drug release from ordered mesoporous silicas. *Current Pharmaceutical Design.* 2015;21;6189-213.
41. Sanz R, Calleja G, Arencibia A, Sans Perez ES. CO<sub>2</sub> uptake and adsorption kinetics of pore-expanded SBA-15 double-functionalized with amino groups. *Energy Fuel.* 2013;27(12):7637-44.
42. Harlick PJE, Sayari A. Applications of pore-expanded mesoporous silica. 5. Triamine grafted material with exceptional CO<sub>2</sub> dynamic and equilibrium adsorption performance. *Ind. Eng. Chem. Res.* 2007;46(2):446-58.



43. Xu X, Song C, Andersen JM, Miller B.G, Scaroni A.W. Novel poly-ethylenimine–modified mesoporous molecular sieve of MCM-41 type as high-capacity adsorbent for CO<sub>2</sub> capture. *Energy Fuels* 2002;16:1463–9.
44. Yıldız MG, Davran Candan T, Günay ME, Yıldırım R. CO<sub>2</sub> capture over amine-functionalized MCM41 and SBA-15: exploratory analysis and decision tree classification of past data. *Journal of CO2 Utilization*. 2019;31:27-42.
45. Sanz R, Calleja G, Arencibia A, Sans Perez ES. CO<sub>2</sub> adsorption on branched polyethyleneimine-impregnated mesoporous silica SBA-15. *Appl Surf Sci*. 2010;256(17):5323-28.
46. Sans Perez ES, Olivarez Marine M, Arencibia A, Sanz R, Calleja G, Maroto Valer MM. CO<sub>2</sub> adsorption performance of amino-functionalized SBA-15 under post-combustion conditions. *Int J Greenh Gas Control*. 2013;17:366-75.
47. Ma X, Wang X, Song C. “Molecular Basket” sorbents for separation of CO<sub>2</sub> and H<sub>2</sub>S from various gas streams. *J Am Chem Soc*. 2009;131(16):5777-83.
48. Wang LF, Yang RT. Increasing selective CO<sub>2</sub> adsorption on amine-grafted SBA-15 by increasing silanol density. *J Phys Chem C*. 2011;115(43):21264-72.
49. Zelenak L, Badanicova M, Halamova D, Cejka J, Zukal A, Murafa N, Goerigk G. Amine-modified ordered mesoporous silica: effect of pore size on CO<sub>2</sub> capture. *Chem Eng J*. 2008;144(2):336-42.
50. Hori K, Tiguchi T, Aoki Y, Miyamoto M, Oumi Y, Yogo K, Uemiya S. Effect of pore size, aminosilane density and aminosilane molecular weight on CO<sub>2</sub> adsorption performance in aminosilane modified mesoporous silica. *Microporous Mesoporous Mater*. 2017;246:158-65.
51. Liu Z, Theng Y, Zhang K, Cao Y, Pan W. CO<sub>2</sub> adsorption properties and thermal stability of different amine-impregnated MCM-41 materials. *J Fuel Chem Technol*. 2013;41(4):469-75.
52. Versteeg GF, van Dijck LAJ, van Swaaij WPM. On the kinetics between CO<sub>2</sub> and alkanolamines both in aqueous and non aqueous solutions: an overview. *Chem Eng Commun*. 1996;144:113-58.

53. Xie HB, Zhou Y, Zhang Y, Johnson JK. Reaction mechanism of monoethanolamine with CO<sub>2</sub> in aqueous solution from molecular modelling. *J Phys Chem A*. 2010;114:11844-52.
54. Iida K, Sato H. Proton transfer step in the carbon dioxide capture by monoethanolamine: a theoretical study at a molecular level. *J Phys Chem B*. 2012;116:2244-8.
55. Davran CT. DFT Modeling of CO<sub>2</sub> interaction with various aqueous amine structures. *J. Phys. Chem. A*. 2014;118:4582–90.
56. Danckwertz PV. The reaction of CO<sub>2</sub> with ethanolamines. *Chem Eng Sci*. 1976;34:443-6.
57. Sartori G, Savage DW. Sterically hindered amines for CO<sub>2</sub> removal from gases. *Ind. Eng. Chem. Fundam*. 1983;22:239–49.
58. da Silva EF, Svendsen H.F. Computational chemistry study of reactions, equilibrium, and kinetics of chemical CO<sub>2</sub> absorption. *Int. J. Greenhouse Gas Control* 2007;1:151–7.
59. Leal O, Bolivar C, Ovalles C, Garcia JJ, Espidel Y. Reversible adsorption of carbon dioxide on amine surface-bonded silica gel. *Inorganica Chimica Acta*. 1995;240:183-9.
60. Huang HY, Yang RT, Chinn D, Munson CL. Amine-grafted MCM-48 and silica xerogel as superior sorbents for acidic gas removal from natural gas. *Ind. Eng. Chem. Res*. 2003;42:2427-33.
61. Chang ACC, Chuang SSC, Gray M, Soong Y. In-situ infrared study of CO<sub>2</sub> adsorption on SBA-15 grafted with  $\zeta$ -(Aminopropyl)triethoxysilane. *Energy & Fuels*. 2003;17:468-73.
62. Khatri RA, Chuang SSC, Soong Y, Gray M. Carbon dioxide capture by diamine-grafted SBA-15: a combined fourier transform infrared and mass spectrometry study. *Ind. Eng. Chem. Res*. 2005;44:3702-08.

63. Khatri RA, Chuang SSC, Soong Y, Gray M. Thermal and chemical stability of regenerable solid amine sorbent for CO<sub>2</sub> capture. *Energy & Fuels*. 2006;20:1514-20.
64. Zheng F, Tran DN, Busche BJ, Fryxell GE, Addleman RS, Zemanian TS, Aardahl CL. Ethylenediamine-modified SBA-15 as regenerable CO<sub>2</sub> sorbent. *Ind. Eng. Chem. Res.* 2005;44:3099-105.
65. Okabayashi H, Shimizu I, Nishio E, O'Connor CJ. Diffuse reflectance infrared Fourier transform spectral study of the interaction of 3-aminopropyltriethoxysilane on silica gel. Behavior of amino groups on the surface. *Colloid and Polymer Science*. 1997;275(8): 744-53.
66. Culler SR, Ishida H, Koenig JL. Structure of silane coupling agents adsorbed on silicon powder. *Journal of Colloid and Interface Science*. 1985;106(2):334-46.
67. Wang X, Schwartz V, Clark JC, Ma X, Overbury SH, Xu X, Song C. Infrared study of CO<sub>2</sub> sorption over "Molecular Basket" sorbent consisting of polyethylenimine-modified mesoporous molecular sieve. *J. Phys. Chem. C*. 2009;113:7260-68.
68. Knöfel C, Martin C, Hornebecq V, Llewellyn PL. Study of carbon dioxide adsorption on mesoporous aminopropylsilane-functionalized silica and titania combining microcalorimetry and in situ infrared spectroscopy. *J. Phys. Chem.* 2009;113:21726-34.
69. Bacsik Z, Ahlsten N, Ziadi A, Zihao G, Garcia Bennett AE, Martin Matute B, Hedin N. Mechanisms and kinetics for sorption of CO<sub>2</sub> on bicontinuous mesoporous silica modified with n-propylamine. *Langmuir*. 2011;27:11118-28.
70. Danon A, Stair PC, Weitz E. FTIR study of CO<sub>2</sub> adsorption on amine-grafted SBA-15: elucidation of adsorbed species. *J Phys Chem C*. 2011;115:11540-9.
71. Pinto ML, Mafra L, Guil JM, Pires J, Rocha J. Adsorption and activation of CO<sub>2</sub> by amine-modified nanoporous materials studied by solid state NMR and CO<sub>2</sub> adsorption. *Chem Mater*. 2011;23:1387-95.
72. Moore JK, Sakwa Novak MA, Chaikittisilp W, Mehta AK, Conradi MS, Jones CW, Hayes SE. Characterization of a mixture of CO<sub>2</sub> adsorption products in

- hyperbranched aminosilica adsorbent by  $^{13}\text{C}$  solid-state NMR. *Environ Sci Technol.* 2015;49:13684-91.
73. Foo GS, Lee JJ, Chen CH, Hayes SE, Sievers C, Jones CW. Elucidation of surface species through in situ FTIR spectroscopy of carbon dioxide adsorption on amine-grafted SBA-15. *Chem Sus Chem* 2017;10:266–76.
74. Aziz B, Zhao G, Hedin N. Carbon dioxide sorbents with propylamine groups-silica functionalized with a fractional factorial design approach. *Langmuir.* 2011;27:3822-34.
75. Cendak T, Sequeira L, Sardo M, Valente A, Pinto ML, Mafra L. Detecting proton transfer in  $\text{CO}_2$  species chemisorbed on amine-modified mesoporous silicas by using  $^{13}\text{C}$  NMR chemical shift anisotropy and smart control of amine surface density. *Chem Eur J.* 2018;24:10136-45.
76. Afonso R, Sardo M, Mafra L, Gomes JRB. Unravelling the structure of chemisorbed  $\text{CO}_2$  species in mesoporous amino silicas: a critical survey. *Environ Sci Tehncol.* 2019;53:2758-67.
77. Gu Y, Li M. Molecular Modeling. *Handbook of Benzoxazine Resins.* 2011:103-110.
78. Broadbelt LJ and Snurr RQ. Applications of Molecular Modeling in Heterogeneous Catalysis Research. *Applied Catalysis A: General.* 2000;200:23-46.
79. Adcock SA and JA. McCammon. Molecular Dynamics: Survey of Methods for Simulating the Activity of Proteins. *Chem. Rev.* 2006;106:1589-1615.
80. Hehre WJ, Radom L, Schleyer PR, Pople JA. *Ab Initio Molecular Orbital Theory.* New York: John Willey and Sons;1986.
81. Cramer CJ. *Essentials of Computational Chemistry Theories and Models.* Minnesota: John Willey and Sons; 2004.
82. Davran-Candan T. Experimental and Computational Study of Selective CO Oxidation Over  $\text{Au}/\text{Al}_2\text{O}_3$  Catalyst. Ph.D. Report. Boğaziçi University, 2011.

83. Bao G, Hu G, Liu D. Numerical Solution of the Kohn-Sham Equation by Finite Element Methods with an Adaptive Mesh Redistribution Technique. *Journal of Scientific Computing*. 2013;55:372-391.
84. Gatti G, Costenaro D, Vittoni C, Paul G, Crocella V, Mangano E, Brandani S, Bordiga S, Cossi M, Marchese L, Bisio C. CO<sub>2</sub> adsorption on different organo-modified SBA-15 silicas: a multidisciplinary study on the effects of basic surface groups. *Phys. Chem. Chem. Phys.* 2017;19:14114-14128.
85. Aziz B, Hedin N, Bacsik Z. Quantification of chemisorption and physisorption of carbon dioxide on porous silica modified by propylamines: Effect of amine density. *Microporous and Mesoporous Materials*. 2012;159:42-49.
86. Yürdürün S. Determination of the lowest-energy structures of amine-modified mesoporous silica adsorbents for CO<sub>2</sub> capture. B.Sc. Report. Yeditepe University, 2019.
87. Frisch MJ, Trucks GW, Schlegel HB, Scuseria GE, Robb MA, Cheeseman JR, et al *Gaussian 16*. Wallingford CT: Gaussian Inc; 2016.
88. Hanwell MD, Curtis DE, Lonie DC, Vandermeersch T, Zurek E, Hutchison GR. Avogadro: An advanced semantic chemical editor, visualization, and analysis platform. *J. Cheminformatics* 2012;4:17.
89. Becke AD. Density-Functional Thermochemistry. III. the role of exact exchange. *Journal of Chemical Physics*. 1993;98:5648-5652.
90. Leach RA. *Molecular Modelling Principles and Applications*. London: Prentice Hall; 2001.
91. Foresman JB, and Frisch A. *Exploring Chemistry with Electronic Structure Methods*, Pittsburgh: Gaussian Inc; 1996.
92. Gatti G, Vittoni C, Costenaro D, Paul G, Mangano E, Brandani S, Marchese L, Bisio C. The influence of particle size of amino-functionalized MCM-41 silicas on CO<sub>2</sub> adsorption. *Phys. Chem. Chem. Phys.* 2017;19:29449.

93. Shimon D, Chen CH, Lee JJ, Didas SA, Sievers C, Jones CW, Hayes SE.  $^{15}\text{N}$  solid state NMR spectroscopic study of surface amine groups for carbon capture: 3-aminopropylsilyl grafted to SBA-15 mesoporous silica. *Environmental Science and Technology*. 2018;52:1488-1495.

